MARCO^{+} lymphatic endothelial cells sequester arboviruses to limit viremia and viral dissemination

Kathryn S. Carpentier[1], Ryan M. Sheridan[2], Cormac J. Lucas[1], Bennett J. Davenport[1], Frances S. Li[1], Erin D. Lucas[1], Mary K. McCarthy[1], Glennys V. Reynoso[3], Nicolas A. May[1], Beth A.J. Tamburini[1,5], Jay R. Hesselberth[2,4], Heather D. Hickman[3], and Thomas E. Morrison[1*]

[1]Department of Immunology and Microbiology, University of Colorado School of Medicine, Aurora, Colorado, 80045 USA

[2]RNA Bioscience Initiative, University of Colorado School of Medicine, Aurora, Colorado, 80045 USA

[3]Viral Immunity and Pathogenesis Unit, Laboratory of Clinical Microbiology and Immunology, National Institutes of Allergy and Infectious Diseases, NIH, Bethesda, Maryland, 20892 USA

[4]Department of Biochemistry and Molecular Genetics, University of Colorado School of Medicine, Aurora, Colorado, 80045, USA.

[5]Department of Medicine, Division of Gastroenterology and Hepatology, University of Colorado Anschutz Medical Campus School of Medicine, Aurora, Colorado, 80045 USA

***Corresponding author and Lead Contact:** Thomas E. Morrison, Ph.D., Professor, Department of Immunology and Microbiology, University of Colorado School of Medicine, 12800 East 19th Avenue, Room P18-9128, Aurora, CO 80045. 303-724-4283 (Office). Email: thomas.morrison@cuanschutz.edu

Abstract

While viremia in the vertebrate host is a major determinant of arboviral reservoir competency, transmission efficiency, and disease severity, immune mechanisms that control arboviral viremia are poorly defined. Here, we identify critical roles for the scavenger receptor MARCO in controlling viremia during arthritogenic alphavirus infections in mice. Following subcutaneous inoculation, alphavirus particles drain via the lymph and are rapidly captured by $MARCO^{+}$ lymphatic endothelial cells (LECs) in the draining lymph node (dLN), limiting viral spread to the bloodstream. Upon reaching the bloodstream, alphavirus particles are cleared from the circulation by MARCO-expressing Kupffer cells in the liver, limiting viremia and further viral dissemination. MARCO-mediated accumulation of alphavirus particles in the dLN and liver is an important host defense mechanism as viremia and viral tissue burdens are elevated in $MARCO^{-/-}$ mice and disease is more severe. These findings uncover a previously unrecognized arbovirus scavenging role for LECs and improve our mechanistic understanding of viremia control during arboviral infections.

Key Words

Arbovirus / Kupffer cells / lymphatic endothelial cells / MARCO / viremia

Introduction

Over the last two decades we have experienced the unanticipated emergence or re-emergence of multiple arboviruses, leading to far-reaching epidemics. In 2004, chikungunya virus (CHIKV), a mosquito-borne alphavirus, re-emerged in the Indian Ocean region and has since infected millions of people in epidemics spanning the globe, including the Americas (Moro *et al*, 2010; Volk *et al*, 2010; Zeller *et al*, 2016). CHIKV and closely related alphaviruses (e.g., Mayaro, o'nyong'nyong (ONNV), and Ross River (RRV) viruses) cause severe arthralgia and arthritis affecting the small joints. These debilitating symptoms can persist for months to years after infection (Borgherini *et al*, 2008; Couturier *et al*, 2012; Rodríguez-Morales *et al*, 2016; Schilte *et al*, 2013), and have severe economic consequences (Cardona-Ospina *et al*, 2015; Soumahoro *et al*, 2011; Vijayakumar *et al*, 2013). In 2007, the previously obscure Zika virus (ZIKV) caused multiple outbreaks in islands of the Pacific Ocean before spreading to the Americas in 2015 (Duffy *et al*, 2009; Metsky *et al*, 2017; Musso *et al*, 2018). This epidemic revealed an unexpected association of ZIKV with severe disease manifestations, including Guillain-Barré syndrome and congenital ZIKV syndrome (Pierson & Diamond, 2018). Because of this, in 2016 the WHO declared the ZIKV outbreak in the Americas a Public Health Emergency of International Concern. These events underscore the ongoing threat that zoonotic arboviruses pose.

Arboviral infections in humans are often the result of spillover from enzootic cycles, and for many arboviruses, humans are a dead-end host. However, some arboviruses sustain human-mosquito-human transmission, including dengue virus (DENV), yellow fever virus (YFV), ZIKV, and CHIKV (Weaver, 2018), which facilitates global emergence through air travel and allows for rapid spread of the virus through urban areas. While there are many determinants of arbovirus urbanization, a key factor is the development of a magnitude and duration of viremia sufficient to support infection of mosquitoes (Weaver, 2018). Beyond influencing reservoir competency and transmission efficiency, viremia also positively correlates with arboviral disease severity (Chow *et al*, 2011; de St Maurice *et al*, 2018; Pozo-Aguilar *et al*, 2014; Vaughn *et al*, 2000; Vuong *et al*,

2020; Waggoner *et al*, 2016). Thus, understanding factors that influence the magnitude and duration of viremia following arboviral infection is of critical importance.

Following the delivery of arboviruses via a mosquito bite, the virus replicates at the site of inoculation before spreading via the lymph to ultimately reach the bloodstream (Johnston *et al*, 2000; MacDonald, 2000). Given this, arboviruses must evade immune defenses in draining lymph nodes (dLNs) to establish a primary viremia. Within the dLN, subcapsular sinus (SCS) macrophages and medullary sinus (MS) macrophages are strategically positioned to encounter lymph-borne pathogens (Bellomo *et al*, 2018). These cells have been described as molecular "flypaper" given their roles in rapidly capturing a wide range of incoming particulate antigen, including lymph-borne virions (Farrell *et al*, 2015; Junt *et al*, 2007). Moreover, viral replication within SCS macrophages initiates interferon production and facilitates recruitment and activation of immune cells to limit further viral dissemination (Iannacone *et al*, 2010; Kastenmuller *et al*, 2012).

Upon reaching the bloodstream, virus particles must evade clearance by blood-filtering organs to maintain viremia and disseminate to distal tissues. The liver and spleen contain phagocytic cells strategically positioned to recognize and remove circulating self and non-self molecules. In the splenic marginal zone, marginal zone (MZM) and metallophilic (MMM) macrophages remove circulating apoptotic cells, antigen and microbes (Borges da Silva *et al*, 2015; Lewis *et al*, 2019). In the liver, Kupffer cells (KCs), which account for 80-90% of all tissue macrophages (Bilzer *et al*, 2006), line the sinusoids to detect and clear blood-borne microbes and modified host molecules from the circulation (Hickey & Kubes, 2009; Lee *et al*, 2010; Zeng *et al*, 2016).

In prior studies, we found that i.v. inoculated arthritogenic alphavirus virions were rapidly removed from the circulation and accumulated in the liver (Carpentier *et al*, 2019). In addition, we identified the scavenger receptor MARCO as essential for alphavirus particle clearance from the blood (Carpentier *et al*., 2019). These findings revealed a critical host defense mechanism that

92 contributes to the control of arbovirus viremia once viral particles have reached the bloodstream.
93 Here, using genetic approaches, confocal microscopy, and single cell mRNA sequencing (scRNA-
94 seq) analysis of dLN cell populations, we expand these analyses to improve our mechanistic
95 understanding of the role of MARCO during arthritogenic alphavirus infection following a more
96 natural subcutaneous inoculation route. Our studies revealed two distinct roles for MARCO in
97 controlling arthritogenic alphavirus dissemination in vertebrate hosts. First, MARCO^{+} LECs in the
98 dLN sequester CHIKV particles to delay the establishment of viremia. Once this barrier is
99 breached, MARCO-expressing Kupffer cells in the liver provide a second layer of protection by
100 removing circulating viral particles. These findings advance our understanding of the immune
101 mechanisms that control arthritogenic alphavirus viremia and dissemination and reveal an
102 arbovirus-scavenging role for LECs.

Results

CHIKV infection outcomes are more severe in MARCO$^{-/-}$ mice.

To further elucidate the role of MARCO during arthritogenic alphavirus infection, we inoculated four-week-old WT or MARCO$^{-/-}$ mice subcutaneously (s.c.) in the left rear footpad with CHIKV and evaluated disease outcomes. As a control, WT and MARCO$^{-/-}$ mice were inoculated with CHIKV E2 K200R, a mutant virus that evades MARCO-mediated clearance from the circulation (Carpentier *et al.*, 2019) and causes severe disease in WT mice (Hawman *et al*, 2017). WT mice inoculated with WT CHIKV steadily gained weight (**Fig 1A**) and displayed little to no defects in gait or hind-limb gripping ability (**Fig 1B**). In contrast, and similar to previous findings (Hawman *et al.*, 2017), WT mice inoculated with CHIKV E2 K200R had delayed weight gain and developed more severe signs of musculoskeletal disease. Similarly, MARCO$^{-/-}$ mice infected with either WT CHIKV or CHIKV E2 K200R developed more severe disease signs (**Fig 1A and 1B**). Notably, the disease observed in MARCO$^{-/-}$ mice infected with CHIKV E2 K200R was not more severe than disease in MARCO$^{-/-}$ mice infected with WT CHIKV, suggesting that the enhanced disease caused by CHIKV E2 K200R in WT mice is due to evasion of MARCO. These findings demonstrate that the scavenger receptor MARCO protects from severe CHIKV disease.

CHIKV viremia and tissue burdens are elevated in MARCO$^{-/-}$ mice

Since our previous work identified a critical role for MARCO in clearing arthritogenic alphavirus particles from the circulation (Carpentier *et al.*, 2019), we evaluated the extent to which the magnitude and duration of viremia is altered in MARCO$^{-/-}$ mice. At 1-day post-inoculation (dpi), infectious virus in the blood of MARCO$^{-/-}$ mice was elevated (230-fold; $P < 0.0001$) compared with WT mice (**Fig 1C**). Viremia peaked in both WT and MARCO$^{-/-}$ mice at 2 dpi, but peak viremia was 150-fold higher in MARCO$^{-/-}$ mice. In addition, MARCO$^{-/-}$ mice maintained an elevated level of infectious virus in the serum through day five post-infection (**Fig 1C**). As neutralizing antibody can

mask viral particles in the circulation at later times post-infection, we also analyzed serum samples for viral genomes by RT-qPCR. This analysis revealed that while CHIKV particles were mostly cleared from the blood of WT mice by 7 dpi, they remained detectable in the blood of MARCO$^{-/-}$ mice (**Fig 1D**). These findings demonstrate that in the absence of MARCO both the magnitude and duration of viremia are increased.

We next evaluated whether the presence or absence of MARCO influences viral dissemination by quantifying viral burden in tissues proximal and distal to the inoculation site at 1 dpi. CHIKV burdens were similar in the ipsilateral ankle of WT and MARCO$^{-/-}$ mice, suggesting that MARCO does not influence replication near the site of inoculation (**Fig 1E**). In contrast, MARCO$^{-/-}$ mice had 2-3 orders of magnitude more infectious virus in distal tissues compared with WT mice (contralateral ankle: 3,163-fold, $P < 0.0001$; contralateral quadriceps: 951-fold, $P < 0.0001$) (**Fig 1E**). These findings were not unique to CHIKV, as infection of MARCO$^{-/-}$ mice with two other arthritogenic alphaviruses, ONNV and RRV, also resulted in elevated viral burdens in distal tissues and in the serum at 1 dpi compared with WT mice (**Fig 1F-G**). The elevated viral burden observed in the contralateral ankle and quadriceps of MARCO$^{-/-}$ mice infected with CHIKV persisted throughout the course of infection, with increased viral burden observed at days 3, 7 and 14 post-infection (**Fig S1A-C**). These findings demonstrate that in the absence of MARCO, arthritogenic alphaviruses develop a much higher viremia and are better able to disseminate to distal tissues.

Kupffer cells rapidly remove CHIKV particles from the circulation.

In prior studies, we found that i.v. inoculated CHIKV particles are rapidly cleared from the circulation and accumulate in the liver in a MARCO-dependent manner (Carpentier *et al.*, 2019). Moreover, depletion of phagocytic cells in the spleen and liver in contact with the blood, through i.v. administration of clodronate-loaded liposomes (CLL), prevented accumulation of CHIKV RNA in the liver (Carpentier *et al.*, 2019). These data suggest that KCs play a dominant role in the

removal of CHIKV particles from the circulation. Based on these data, we hypothesized that MARCO-mediated clearance of viral particles by KCs limits the magnitude and duration of viremia, thus restricting viral dissemination and pathogenicity. To test this, we evaluated the extent to which specific depletion of KCs impaired the clearance of circulating CHIKV particles. To do this, we used Clec4F-DTR mice (Scott *et al*, 2016), which express the diphtheria toxin receptor (DTR) under the control of *Clec4f*, a gene expressed exclusively in KCs. We treated WT or Clec4F-DTR$^+$ mice with DT 1-2 days prior to i.v. inoculation of CHIKV. In WT mice, CHIKV particles were rapidly cleared from the circulation by 45 min (**Fig 2A**). In contrast, Clec4F-DTR$^+$ mice had increased viral particles in the serum at this time point (77-fold; $P < 0.0001$) (**Fig 2A**), demonstrating that KCs contribute to CHIKV clearance. However, the block to clearance in DT-treated Clec4F-DTR$^+$ mice was not as robust as observed in mice treated i.v. with CLL (**Fig 2B**). Given the broad effects of CLL treatment (Seiler *et al*, 1997; Van Rooijen & Sanders, 1994), we employed CD169-DTR$^+$ mice (Miyake *et al*, 2007), which allow for specific depletion of CD169$^+$ cells, including liver KCs and splenic MMM and MZM (Gupta *et al*, 2016; Miyake *et al.*, 2007). CHIKV clearance was blocked in DT-treated CD169-DTR$^+$ mice to levels similar to that observed in CLL-treated mice (**Fig 2C**). However, we found that KC depletion was much more efficient in CLL-treated WT mice and DT-treated CD169-DTR$^+$ mice compared with DT-treated Clec4F-DTR$^+$ mice, with averages of 1.25 (CLL), 2.5 (CD169-DTR$^+$) and 11.5 (Clec4F-DTR$^+$) F4/80$^+$ cells per field of view (**Fig 2D-E)**. The less efficient depletion of KCs in Clec4F-DTR$^+$ mice likely accounts for the less potent block to clearance of circulating CHIKV particles. Collectively, these findings suggest that KCs are primarily responsible for the rapid removal of CHIKV from the circulation following i.v. inoculation.

Depletion of KCs is not sufficient to enhance early CHIKV dissemination.

We reasoned that if clearance of viral particles by MARCO-expressing KCs was responsible for the enhanced viremia and dissemination observed in MARCO$^{-/-}$ mice following s.c.

virus inoculation, depletion of KCs would also enhance CHIKV dissemination. To test this idea, we treated WT or Clec4F-DTR^{+} mice with DT prior to s.c. inoculation of CHIKV in the left rear footpad and measured viral burden in tissues at 1 dpi. Surprisingly, unlike what we observed in MARCO$^{-/-}$ mice (**Fig 1E**), the amounts of CHIKV in tissues and the circulation of WT and DT-treated Clec4F-DTR^{+} mice were indistinguishable (**Fig 3A**). Given that depletion of KCs is not complete in DT-treated Clec4F-DTR^{+} mice (**Fig 2D-E**), we i.v. treated WT mice with PLL or CLL 42 h prior to s.c. inoculation of CHIKV in the left rear footpad, as i.v. CLL treatment efficiently depletes F4/80^{+} cells in the liver (**Fig 2D-E**). Despite this, we found that CHIKV levels in distal tissues at 1 dpi were indistinguishable among PLL- and CLL-treated mice (**Fig 3B**). However, viremia was elevated in CLL-treated mice (27-fold; $P < 0.001$) (**Fig 3B**), confirming a role for phagocytic cells in limiting CHIKV viremia. These data demonstrate that while the absence of MARCO is sufficient to enhance CHIKV dissemination, depletion of KCs is not, suggesting that additional MARCO expressing cells restrict CHIKV dissemination.

The draining lymph node limits arthritogenic alphavirus dissemination.

Following replication at the site of inoculation, arthritogenic alphaviruses spread through the lymph to the dLN before establishing viremia and disseminating to distal tissues. Given this, we hypothesized that MARCO-expressing cells in the dLN capture CHIKV particles, delaying the establishment of viremia and limiting viral dissemination to distal tissues. To test this, we used lymphotoxin alpha deficient mice (LT$\alpha^{-/-}$), which developmentally lack peripheral lymph nodes (De Togni *et al*, 1994). To evaluate the relative contributions of the dLN and liver in controlling CHIKV dissemination, WT or LT$\alpha^{-/-}$ mice were treated i.v. with PLL or CLL to deplete phagocytic cells in the liver prior to s.c. inoculation of CHIKV in the left rear footpad. At 1 dpi, the viral burden in tissues proximal and distal to the site of inoculation were quantified. In WT mice, low levels of virus were detected in distal tissues and serum of both PLL- and CLL-treated mice (**Fig 4A**). In

contrast, PLL-treated LT$\alpha^{-/-}$ mice, which lack LNs but retain liver KCs, had an elevated viral burden in distal muscle (29-fold; $P < 0.0001$) and joint tissue (107-fold; $P < 0.0001$), and had moderately elevated viremia (10-fold; $P < 0.0001$) (**Fig 4A**). Compared with PLL-treated LT$\alpha^{-/-}$ mice, LT$\alpha^{-/-}$ mice treated with CLL, which lack both LNs and KCs, had higher viral burdens in distal muscle (4-fold; $P < 0.05$) and joint tissue (7-fold; $P < 0.0001$), and a highly elevated viremia (223-fold; $P < 0.0001$) (**Fig 4A**). These findings demonstrate that the dLN functions as a major barrier to CHIKV dissemination, as in its absence viral dissemination to distal tissues is strongly increased. The modest elevation in viremia in PLL-treated LT$\alpha^{-/-}$ mice compared with CLL-treated LT$\alpha^{-/-}$ mice suggests that phagocytic cells in the liver remove much of the circulating virus. An important role for liver phagocytes in controlling dissemination is supported by the elevated viral burden in both distal tissues and the circulation in CLL-treated LT$\alpha^{-/-}$ mice, which lack both LNs and KCs (**Fig 4A**).

The enhanced viral dissemination observed in CLL-treated LT$\alpha^{-/-}$ mice (**Fig 4A**) is similar to what was observed in MARCO$^{-/-}$ mice (**Fig 1E**), suggesting that MARCO-expressing cells in the dLN sequester alphavirus particles. To explore this idea, we inoculated WT or MARCO$^{-/-}$ mice s.c. in the footpad with WT CHIKV or CHIKV E2 K200R (mutant virus that evades MARCO). At 2 hpi, a time point at which no new infectious virus has been produced, we collected the dLN and serum to evaluate the fate of the inoculated virus. In WT mice inoculated with WT CHIKV, we detected high levels of viral RNA in the dLN, while little to no virus was observed in the serum (**Fig 4B**). In contrast, WT mice inoculated with CHIKV E2 K200R and MARCO$^{-/-}$ mice inoculated with either WT CHIKV or CHIKV E2 K200R had 7-10-fold lower levels of viral RNA in the dLN, and remarkably had 3,700-6,200-fold more virus in the serum (**Fig 4B**). Moreover, we found that MARCO$^{-/-}$ mice inoculated with RRV, a closely related arthritogenic alphavirus, also had reduced viral RNA in the dLN (5-fold; $P < 0.001$) and higher levels of virus in the blood (1,790-fold; $P < 0.0001$) compared with WT mice (**Fig 4C**). Importantly, MARCO$^{-/-}$ mice inefficiently clear

231 circulating viral particles (Carpentier *et al.*, 2019). Therefore, the increased viremia in MARCO$^{-/-}$
232 mice 2 h following s.c. virus inoculation is likely a reflection of not only reduced virus accumulation
233 in the dLN, but also the lack of clearance of circulating virus by liver KCs.
234
235 **LN Macrophages are not required for CHIKV accumulation in the dLN or for limiting viral**
236 **dissemination**
237 We next sought to define the cell type(s) in the dLN that limit CHIKV dissemination. Within
238 the LN, MARCO is reported to be expressed by MS macrophages (Elomaa *et al*, 1995) and a
239 subset of LECs in the medullary region (Fujimoto *et al*, 2020; Takeda *et al*, 2019; Walsh *et al*,
240 2021; Xiang *et al*, 2020). Consistent with these data, using flow cytometry we found that MARCO
241 was expressed specifically on MS macrophages and LECs (**Fig S2**). Previous studies found that
242 macrophages in the dLN capture lymph-borne viruses (Farrell *et al.*, 2015; Gonzalez *et al*, 2010;
243 Hickman *et al*, 2008; Junt *et al.*, 2007), and that CLL-mediated depletion of dLN macrophages
244 decreased viral capture by the dLN and increased viremia and dissemination (Farrell *et al.*, 2015;
245 Junt *et al.*, 2007). Given this, we hypothesized that MARCO^{+} MS macrophages limit the
246 dissemination of arthritogenic alphaviruses. As MS and SCS macrophages in the LN are CD169^{+}
247 (Gray & Cyster, 2012), we used CD169-DTR mice to deplete LN macrophages and evaluate their
248 capacity to promote virus accumulation in the dLN and limit virus accumulation in the circulation.
249 WT or CD169-DTR mice were treated with DT, which results in efficient depletion of CD169^{+} cells
250 in the dLN (**Fig 5A**). Mice were then inoculated with CHIKV s.c. in the footpad and at 2 hpi, viral
251 RNA in the dLN and serum was quantified by RT-qPCR. Remarkably, there was no difference in
252 the amount of viral RNA detected in the dLN of DT-treated WT or CD169-DTR^{+} mice, and low
253 levels of viral RNA in the blood were observed in both WT and CD169-DTR^{+} mice (**Fig 5B**).
254 Importantly, DT treatment of CD169-DTR mice also depletes KCs (**Fig 2D and 3E**), and thus any
255 virus that traffics from the dLN to the blood should remain circulating and not be masked by the
256 clearance effects of KCs. These findings suggest that macrophages in the dLN are not required

to sequester viral particles and limit access to the circulation. Consistent with this, CHIKV dissemination to distal tissues was not enhanced in DT-treated CD169-DTR^{+} mice compared with WT mice (**Fig 5C**), or in mice treated with CLL both i.v. and s.c. in the footpad to deplete phagocytic cells in the liver and dLN, respectively (**Fig S3**). These findings reveal that in contrast to previous reports for other viruses (Junt *et al.*, 2007), LN macrophages are not required for clearance of arthritogenic alphavirus particles from the lymph.

CHIKV-E2-mCherry particles co-localize with MARCO^{+} LECs in the dLN

Given that medullary macrophages are not required for accumulation of arthritogenic alphavirus particles in the dLN, we next investigated the role of LECs, as recent reports identified a subset of LECs in the medullary region of the lymph node that express MARCO (Fujimoto *et al.*, 2020; Xiang *et al.*, 2020). Moreover, LECs have been shown to capture and archive viral antigen (Tamburini *et al*, 2014), further supporting a potential role for LECs in capturing alphavirus particles. To determine whether viral particles colocalized with MARCO^{+} LECs in the dLN, we used a recombinant CHIKV in which mCherry is fused to the E2 glycoprotein present in viral particles (CHIKV-E2-mCherry). Importantly, CHIKV-E2-mCherry particles were efficiently cleared from the circulation, and clearance could be blocked by pre-treatment of mice with poly(I), a class A SR inhibitor that competitively inhibits MARCO (Chen *et al*, 2006) (**Fig S4**). CHIKV-E2-mCherry particles were inoculated s.c. into the foot and the popliteal dLN was collected at 2 hpi. Frozen LN sections were stained for Lyve1^{+} LECs, MARCO, B220 (marking B cell follicles and revealing nodal orientation) and mCherry^{+} CHIKV particles. As previously reported, we detected a robust MARCO^{+} Lyve1^{+} LEC population in both infected and uninfected WT mice that was primarily restricted to the LN medullary sinus (**Fig 6A**). Although MARCO$^{-/-}$ mice lacked MARCO^{+} cells as expected, the medullary sinus remained intact with similar morphology to that of WT mice (**Fig 6A**, middle panels). Visually, mCherry staining for CHIKV particles was most intense in Lyve1^{+} MARCO^{+} LECs (**Fig 6A**, far right panels). To better quantify CHIKV^{+} cells in the LECs of WT and

MARCO$^{-/-}$ mice, we first colocalized mCherry and Lyve1^{+} signals in the LN, detecting many double positive cells in WT but not MARCO$^{-/-}$ LNs (**Fig 6B-C**). Indeed, while 39.3% of Lyve1^{+} voxels in were also mCherry^{+} in WT LNs, only 3.0 % were mCherry^{+} in MARCO$^{-/-}$ mice, consistent with the decreased accumulation of viral genomes in the dLN of MARCO$^{-/-}$ mice at 2 hpi (**Fig 5B**). Higher magnification images demonstrated that in WT mice, mCherry staining overlapped with both Lyve1 and MARCO staining (**Fig 6D**). In contrast, in MARCO$^{-/-}$ LNs, we observed only a small amount of mCherry staining in CD11b^{+} cells, some of which co-expressed CD169 (representing medullary sinus macrophages) (**Fig 6E**). Collectively, these findings demonstrate that following s.c. inoculation, CHIKV particles are bound by medullary sinus LECs using MARCO$^{-/-}$.

MARCO^{+} LECs harbor CHIKV RNA

To further characterize LEC subsets that capture virus, at 24 hpi we generated single cell suspensions from the dLN for three biological replicates each of mock- and CHIKV-infected mice. We then enriched for CD45^{-} cells (**Fig S5**) and performed scRNA-seq to identify cell populations that harbor viral RNA. Between mock- and CHIKV-infected samples, which clustered distinctly, we captured a total of 60,185 cells (**Fig 7A**). To identify the cell types represented in these samples, we used an automated approach (Fu *et al*, 2020) that classifies cells based on their correlation with reference RNA-seq data. Using published data for cell types found in the mouse LN (Heng, 2008; Malhotra *et al*, 2012; Rodda *et al*, 2018), we were able to identify large populations of endothelial cells, non-endothelial stromal cells including fibroblastic reticular cells (FRC) and perivascular cells (PvC), along with smaller populations of CD45^{+} cells including B cells, T cells, and macrophages (**Fig 7B**). To identify endothelial cell subsets, we further divided the endothelial cells into niche-specific subpopulations using published reference data (Xiang *et al.*, 2020). By this method, we identified blood endothelial cells (BEC) as well as LEC subsets including MARCO^{+}, ceiling (cLEC), floor (fLEC), valve, collecting, Ptx3, and transition zone (tzLEC) (**Fig 7C and EV6**). Cells collected from the dLN of CHIKV-infected mice contained fewer

LEC subsets and were mainly composed of MARCO$^+$ LECs, valve LECs, and a population of endothelial cells that we were unable to further classify (**Fig 7C**). The limited number of LEC subsets identified in CHIKV-infected samples could be due to cell death within the dLN at 24 hpi. However, one caveat to our approach is that we are using reference data from uninfected mice which could make it more challenging to accurately annotate LN cell populations during CHIKV infection.

To identify cell types harboring CHIKV RNA, we classified cells based on the number of viral sequence counts. As expected, we detected only background levels of CHIKV RNA (3/26,500 cells with 1 CHIKV count each) in dLN cells of mock-infected mice (**Fig S7A**), while cells collected from the dLN of CHIKV-infected mice had viral RNA sequence counts as high as >8,000 per cell (**Fig S7A**). We used k-means clustering to divide cells from each sample into CHIKV-low and CHIKV-high groups and identified a small number of cells (n = 690, 1.1%) with high amounts of CHIKV RNA (**Fig S7A**). CHIKV-high cells displayed fewer mouse mRNA counts per cell and fewer expressed mouse genes (**Fig S7B**) potentially due to inhibition of host cell transcription or cell lysis, both of which can occur in CHIKV-infected cells (Fros & Pijlman, 2016).

We next analyzed the cell populations containing high amounts of CHIKV RNA. CHIKV-high cells are mainly composed of MARCO$^+$ LECs (n = 231, 33%), FRCs (n = 89, 13%), BECs (n = 49, 7%), and PvCs (n = 44, 6%), along with a group of LECs that we were unable to further classify (unassigned-LEC, n = 232, 34%) (**Fig 7F**). Among the CHIKV-high cell types, we found that the unassigned-LECs and MARCO$^+$ LECs show the highest viral burden as indicated by a high fraction of CHIKV counts per cell (**Fig 7E-G**), suggesting that these are the predominant cell populations in the dLN that capture viral particles. To further investigate the role of MARCO in these interactions, we compared MARCO expression for CHIKV-low and CHIKV-high MARCO$^+$ LECs. This analysis revealed that CHIKV-high MARCO$^+$ LECs had significantly higher expression of MARCO in comparison to their CHIKV-low counterparts (**Fig 7D and 7H**). Moreover, CHIKV-low and CHIKV-high MARCO$^+$ LECs expressed little to no Mxra8, a cell entry receptor for CHIKV

335 (Zhang *et al*, 2018) (**Fig 7I**). These data further support a role for MARCO and LECs in
336 sequestering viral particles in the dLN and limiting CHIKV dissemination.
337
338 **Discussion**
339 Our results reveal a critical role for the scavenger receptor MARCO in controlling
340 arthritogenic alphavirus viremia, dissemination, and disease. Similar protective roles for MARCO
341 have been observed during other infections. For example, MARCO$^{-/-}$ mice are impaired in their
342 ability to clear *Streptococcus pneumonia* from the nasopharynx and lungs (Arredouani *et al*, 2004;
343 Dorrington *et al*, 2013). Moreover, MARCO enhances phagocytosis of *Mycobacterium*
344 *tuberculosis in vitro* (Bowdish *et al*, 2009), and MARCO polymorphisms are associated with
345 altered susceptibility to pulmonary tuberculosis (Bowdish *et al*, 2013; Lao *et al*, 2017; Ma *et al*,
346 2011; Thuong *et al*, 2016). Finally, during influenza A virus infection in mice, MARCO suppresses
347 early immunopathologic inflammatory responses, and accordingly, MARCO$^{-/-}$ mice have
348 increased morbidity and mortality compared with WT mice (Ghosh *et al*, 2011). However, MARCO
349 also can be exploited by pathogens. For example, herpes simplex virus 1 (HSV-1) interactions
350 with MARCO enhance epithelial cell adsorption, and MARCO$^{-/-}$ mice have reduced wound sizes
351 following s.c. HSV-1 inoculation (MacLeod *et al*, 2013).
352 Our findings identify two distinct MARCO expressing cell types that limit arthritogenic
353 alphavirus dissemination and viremia: MARCO^{+} LECs in the dLN and KCs in the liver. KCs are
354 well established to play a critical role in controlling bacteremia (Jenne & Kubes, 2013; Lee *et al.*,
355 2010) However, the role of KCs in controlling viremia is not as well characterized. We find that
356 specific depletion of KCs using Clec4F-DTR^{+} mice impairs CHIKV clearance from the circulation.
357 While it remains possible that MARCO^{+} MZM in the spleen contribute, our findings demonstrate
358 that KCs are the major cell type involved in the efficient removal of arthritogenic alphavirus
359 particles from the blood, expanding their surveillance function to arboviruses.

Despite the critical role for KCs in removing alphavirus particles from the circulation, we found that depletion of KCs had no impact on CHIKV dissemination following s.c. viral inoculation. This led us to investigate the role of MARCO$^+$ cells in the dLN in controlling CHIKV viremia and dissemination, as lymph nodes can function as barriers to pathogen dissemination (Bogoslowski & Kubes, 2018). For example, within minutes of subcutaneous inoculation, fluorescently labeled vesicular stomatitis virus (VSV) particles can be found trapped within SCS macrophages in the dLN (Junt *et al.*, 2007). This observation extends to other viruses, including adenovirus (AdV) and vaccinia virus (VV) (Hickman *et al.*, 2008; Junt *et al.*, 2007), thus lending to the description of these SCS macrophages as "molecular flypaper" in regard to their ability to capture incoming viral particles. This macrophage-mediated capture has important implications for pathogen dissemination, as depletion of macrophages in the draining lymph node via s.c. CLL administration decreased accumulation of VSV in the dLN at early times post-infection, and increased viral dissemination to the blood (Junt *et al.*, 2007). Similarly, depletion of macrophages in the dLN was shown to enhance the dissemination of murine cytomegalovirus (MCMV), West Nile virus (WNV), and *Pseudomonas aeruginosa (P. aeruginosa)*, and facilitate CNS invasion of neurotropic VSV (Farrell *et al.*, 2015; Iannacone *et al.*, 2010; Kastenmuller *et al.*, 2012; Winkelmann *et al*, 2014).

Our results demonstrate the dLN is a major barrier to arthritogenic alphavirus dissemination, but unlike prior reports of macrophage-mediated capture our findings uncover a previously unrecognized role for LECs in scavenging arboviral particles to impair dissemination. We found that CHIKV-E2-mCherry particles colocalized with MARCO$^+$ LECs in the dLN, and scRNA sequencing of dLN stromal cell populations identified MARCO$^+$ LECs as the predominant cell type harboring CHIKV RNA. Notably, CHIKV RNA levels among MARCO$^+$ LECs correlated with MARCO expression levels, with CHIKV-high cells showing higher expression of MARCO, suggesting MARCO may mediate internalization. MARCO$^+$ LECs were negative for *Mxra8*, a known arthritogenic alphavirus entry receptor (Zhang *et al.*, 2018). The genetic absence of *Mxra8*

386 in mice reduced but did not eliminate viral replication and dissemination *in vivo* (Zhang *et al*,
387 2019), demonstrating that additional entry receptors exist. Notably, MARCO has been reported
388 to facilitate entry of other viruses, including HSV-1, VV, and adenovirus into target cells (MacLeod
389 *et al*, 2015; MacLeod *et al.*, 2013; Maler *et al*, 2017; Stichling *et al*, 2018).

390 The role of LECs in capturing lymph-borne viral particles likely extends beyond
391 arthritogenic alphaviruses. While macrophages were reported to play a major role in capture of
392 other viruses, fluorescently labeled VSV, AdV, and VV particles co-localized with LECs in the
393 medullary region of the dLN (Junt *et al.*, 2007; Reynoso *et al*, 2019), which is where MARCO$^+$
394 LECs reside. Future investigations are needed to understand whether MARCO is responsible for
395 broadly mediating capture of diverse viruses by LECs, or whether other pattern recognition
396 receptors (PRRs) are also involved. LECs express a wide range of PRRs, including toll-like
397 receptors, Fc receptors, C-type lectin receptors, and additional scavenger receptors, suggesting
398 they may have multiple mechanisms for scavenging diverse viral particles (Berendam *et al*, 2019;
399 Jalkanen & Salmi, 2020).

400 Additional work is also needed to better understand the consequences of viral capture by
401 LECs. Our findings suggest that capture of arthritogenic alphaviruses by MARCO$^+$ LECs
402 contributes to the control of viral dissemination. However, whether LECs become productively
403 infected by arthritogenic alphaviruses remains under investigation. In prior studies, we were
404 unable to detect fluorescent signal in the dLN following s.c. inoculation with a recombinant CHIKV
405 expressing the fluorescent protein mKate (McCarthy *et al*, 2018). However, our scRNA-seq
406 results reveal that only a small fraction of stromal cells in the dLN harbor CHIKV RNA, suggesting
407 flow cytometry may not be sensitive enough to detect whether the virus is productively replicating
408 in these cells. Our scRNA-seq analysis provides hints that the MARCO$^+$ LECs may be actively
409 infected. For example, cells harboring CHIKV RNA have high viral reads, suggestive of genome
410 replication, and CHIKV-high cells have reduced reads for mouse genes, which is consistent with
411 virus-mediated transcriptional shutoff (Fros & Pijlman, 2016). Further studies are needed, but

412 these findings raise the possibility that MARCO facilitates arthritogenic alphavirus entry and
413 infection of distinct cell types, such as MARCO$^+$ LECs.

414 LEC-mediated capture of viral particles also could influence innate and adaptive immune
415 responses. LECs have been reported to archive viral antigen for weeks following the resolution
416 of the adaptive immune response (Kedl *et al*, 2017; Tamburini *et al.*, 2014), and our findings may
417 provide insight as to how these antigens are initially acquired by LECs. This archived antigen can
418 be either directly presented or exchanged with dendritic cells to allow for cross-presentation to
419 CD8$^+$ T-cells to stimulate memory T cells and augment protective immunity (Kedl *et al.*, 2017;
420 Tamburini *et al.*, 2014; Vokali *et al*, 2020). In other studies evaluating factors that influence
421 alphavirus viremia and dissemination, injection of Semliki Forest virus, a closely related
422 alphavirus, at the site of a mosquito bite in the skin of mice was found to delay viral spread to the
423 lymph node, which ultimately enhanced early viremia and viral dissemination, and led to more
424 severe disease outcomes (Pingen *et al*, 2016). It is possible that the retention of viral particles at
425 the site of inoculation allows the virus to replicate to high titers before initiating potent immune
426 responses due to viral capture in the dLN. Future studies are necessary to better understand how
427 MARCO$^+$ LEC-mediated capture of arthritogenic alphaviruses influences downstream innate and
428 adaptive immune responses.

429 In summary, our results reveal a critical scavenging role for MARCO during arthritogenic
430 alphavirus infection. We find that following s.c. inoculation, alphavirus particles accumulate in the
431 dLN in association with MARCO$^+$ LECs, limiting viral spread to the blood. Once reaching the
432 blood, liver KCs provide a second line of defense and rapidly clear circulating alphavirus particles
433 in a MARCO-dependent manner. Collectively, these findings advance our mechanistic
434 understanding of how viremia is controlled during arboviral infections, which has several important
435 implications for arboviral biology. First, viremia has been shown to positively correlate with
436 disease severity following infection with CHIKV and other arboviruses (Chow *et al.*, 2011; de St
437 Maurice *et al.*, 2018; Pozo-Aguilar *et al.*, 2014; Vaughn *et al.*, 2000; Vuong *et al.*, 2020; Waggoner

438 *et al.*, 2016). Consistent with this, we find that the high magnitude and duration of viremia
439 observed in CHIKV-infected MARCO$^{-/-}$ mice promoted more rapid viral dissemination, increased
440 viral tissue burdens, and resulted in more severe disease signs. These finding raise the possibility
441 that MARCO also influences disease severity in humans. The MARCO gene is highly polymorphic
442 in humans and mice (Bowdish & Gordon, 2009), and this genetic variation has been demonstrated
443 to influence human susceptibility to tuberculosis and respiratory syncytial virus (Bowdish *et al.*,
444 2013; High *et al*, 2016; Lao *et al.*, 2017; Ma *et al.*, 2011; Thuong *et al.*, 2016). Given our findings,
445 it is possible that MARCO polymorphisms similarly influence disease severity following
446 arthritogenic alphavirus infection. In addition to influencing disease severity, MARCO-virus
447 interactions likely also affect virus transmission efficiency and reservoir host competency in
448 nature, as the magnitude and duration of viremia is an important factor dictating which vertebrate
449 species can serve as reservoirs for arboviruses (Weaver, 2018). Thus, differences in MARCO
450 alleles may influence which vertebrate hosts participate in arthritogenic alphavirus transmission
451 cycles. While humans are dead-end hosts for most arboviruses, a select few including CHIKV,
452 DENV, and ZIKV generate a sufficiently high level of viremia to facilitate human-mosquito-human
453 transmission cycles (Weaver, 2018). These viruses pose a high risk for emergence and re-
454 emergence, as evidenced by the now global distribution of DENV and the recent ZIKV and DENV
455 epidemics. This underscores the need for an improved understanding of viremic control.
456 Collectively, our findings shed light on the mechanistic control of viremia during arboviral
457 infections, and more broadly advance our understanding of how the lymph node restricts virus
458 dissemination.
459
460 **Materials and Methods**
461
462 **Ethics Statement.** This study was performed in strict accordance with the
463 recommendations in the Guide for the Care and Use of Laboratory Animals of the National

Institutes of Health. All of the animals were handled according to approved institutional animal care and use committee (IACUC) protocols (#00026) of the University of Colorado School of Medicine (Assurance Number A3269-01). Experimental animals were humanely euthanized at defined endpoints by exposure to isoflurane vapors followed by thoracotomy.

Cells. Vero cells (ATCC CCL81) were cultured at 37°C in Dulbecco's Modified Eagle medium (DMEM)-F-12 (Gibco) supplemented with 10% fetal bovine serum, 1x nonessential amino acids (Life Technologies), and 1X penicillin-streptomycin. BHK-21 cells (ATCC CCL10) were cultured at 37°C in α-minimum essential medium (Gibco) supplemented with 10% FBS, 10% tryptone phosphate broth, and penicillin-streptomycin.

Viruses. The CHIKV strain used in these studies is AF15561, an Asian genotype strain isolated from a human patient in Thailand (GenBank accession no. EF452493). cDNA clones of AF15561 and AF15561 E2 K200R have been described previously (Hawman *et al.*, 2017). The recombinant CHIKV AF15561 cDNA clone encoding mCherry-tagged E2 glycoprotein was derived from a 181/25 CHIKV E2 mCherry-tagged cCNA clone kindly provided by Richard Kuhn (Purdue University). Site-directed mutagenesis was first used to revert positions E2 12 and E2 84 from attenuated 181/25 to WT AF15561 using the following primers: CHIKV-181/25 E2 I12T FOR (5′-gtgagctaggtacggtcttgtggctttatagacattgaa-3′), CHIKV-181/25 E2 I12T REV (5′-ttcaatgtctataaagccacaagaccgtacctagctcac-3′), CHIKV 181/25 E2 R82G FOR (5′-gttcttacaaatagcccggccctctctgcgtc-3′) and CHIKV 181/25 R82G Rev (5′-gacgcagagagggccgggctatttgtaagaac-3′). A fragment containing part of capsid, mCherry, and part of E2 was then subcloned into an AF15561 cDNA clone using restriction sites XhoI and XmaI. To generate virus stocks, linearized cDNA clones were *in vitro* transcribed with SP6 RNA polymerase, and viral RNA was electroporated into BHK-21 cells as described previously

(Ashbrook *et al*, 2014). At 24-28 h post-electroporation, clarified supernatant containing infectious virus was collected, aliquoted and stored at -80°C. The RRV strain used is SN11 (Liu *et al*, 2011), a clinical isolate (kindly provided by John Aaskov, Queensland University of Technology) that was passaged 1X on C6/36 cells before we propagated the stock used in these studies in BHK-21 cells. ONNV SG650 (Lanciotti, 1998), a strain isolated from human sera in Uganda in 1996, was derived from a cDNA clone ((Vanlandingham, 2006); provided by Stephen Higgs, Kansas State University) through electroporation into BHK-21 cells, and propagated on BHK-21 cells for one passage to increase titer. Infectious virus was titered by plaque assay on BHK-21 cells. To quantify viral genomes, viral stocks were treated with RNase1 at 37°C for 1 h. RNA was extracted and viral genomes were quantified by RT-qPCR.

Mouse Experiments. WT C57BL/6 and congenic Lymphotoxin alpha$^{-/-}$ (LT$\alpha^{-/-}$) mice (De Togni *et al.*, 1994) were obtained from the Jackson Laboratory. Congenic CD169-DTR^{+} (Miyake *et al.*, 2007) mice were provided by Jason Cyster (University of California San Francisco) and congenic MARCO$^{-/-}$ mice (Arredouani *et al.*, 2004) were provided by Dawn Bowdish (McMaster University). Clec4F-DTR^{+} C57BL/6 mice (Scott *et al.*, 2016) were provided by Martin Guilliams (Ghent University). CD169-DTR^{+}, MARCO$^{-/-}$, LT$\alpha^{-/-}$ and Clec4F-DTR^{+} mice were housed and bred at the University of Colorado School of Medicine under specific pathogen-free conditions and were distributed randomly into groups containing approximately even division of sexes for experiments. WT male mice were purchased commercially and were age matched and distributed randomly across groups. Mice 4 weeks of age were used in all experiments. All mouse experiments were performed under animal biosafety level 2 or 3 conditions, as appropriate.

For experiments involving Clec4F-DTR^{+} mice, mice were treated with 50 ng of DT either i.v. or i.p. as indicated in the Figure legend, 48 h and 24 h prior to virus inoculation. For experiments involving CD169-DTR^{+} mice, mice were injected with 100 ng of DT i.p. 48 h and 24

h prior to virus inoculation. For experiments involving depletion of liver and splenic phagocytes, mice were inoculated i.v. with 100 μl per 10 g of body weight of PBS- (PLL) or clodronate-loaded liposomes (CLL) (clodronateliposomes.org) 42 h prior to virus inoculation. To deplete phagocytic cells in the draining lymph node, mice were inoculated s.c. in the left-rear footpad with 20 μl of PLL or CLL 24 h prior to virus inoculation.

In experiments evaluating disease or viral tissue burdens, mice were anesthetized with isoflurane vapors and inoculated in the left-rear footpad with a 10 μl volume containing 10^3 PFU of virus diluted in PBS/1% FBS. Mice were weighed daily and disease scores were assigned as described previously (Jupille *et al*, 2011). In brief, the following criteria were used: score of 1: mild deficit in hind paw gripping of injected foot; score of 2: mild deficit in bilateral hind-paw gripping; score of 3: bilateral loss of gripping ability; score of 4: bilateral loss of griping ability, moderate bilateral hind-limb paresis, altered gait, difficulty righting self; score of 5: bilateral loss of gripping ability, severe bilateral hind-limb paresis, altered gait, inability to right self; score of 6: moribund state. At experiment termination, mice were euthanized by exposure to isoflurane vapors followed by bilateral thoracotomy. Blood was collected, mice were perfused with 5-10 mL of 1X PBS or 4% paraformaldehyde (PFA) (for experiments involving histology), and indicated tissues were harvested in *in vitro* diluent (1X PBS with 1% FBS and 1x $Ca^{2+}Mg^{2+}$) for analysis of infectious virus by focus formation assay (FFA) or plaque assay, or in TRIzol reagent Life Technologies) for RNA isolation and quantification of viral genomes by RT-qPCR. Tissues were homogenized using a MagNA Lyser instrument (Roche).

For serum clearance experiments, mice were anesthetized with isoflurane vapors and inoculated i.v. with 10^8 genomes of CHIKV diluted in 100 μl of PBS/1% FBS. At 45 min post inoculation, mice were sacrificed and serum was collected. For lymph node accumulation experiments, mice were anesthetized with isoflurane vapors and inoculated s.c. in the left-rear

538 footpad with a 10 μl volume containing 5 x 10^4 PFU of virus. At 2 hpi, blood and the draining pLN
539 were collected in TRIzol.
540
541 **Viral Genome Quantification by RT-qPCR.** To quantify viral genomes, RNA was
542 extracted from 20 μl of serum or from homogenized tissues in TRIzol reagent using the PureLink
543 RNA mini kit (Life Technologies). CHIKV cDNA was generated from 10 μl of serum derived RNA
544 or 1 μg of tissue derived RNA using random primers (Invitrogen) with SuperScript IV reverse
545 transcriptase (Life Technologies). CHIKV genome copies were quantified by RT-qPCR using a
546 CHIKV specific forward primer (5′-TTTGCGTGCCACTCTGG-3′) and reverse primer (5′-
547 CGGGTCACCACAAAGTACAA-3′) with an internal TaqMan probe (5′-
548 ACTTGCTTTGATCGCCTTGGTGAGA-3′), as previously described (Hawman *et al*, 2013). RRV
549 cDNA was generated from 10 μl of serum derived RNA or 1 μg of tissue derived RNA using a
550 sequence-tagged (indicated with lower case letters) RRV-specific RT primer (5′-
551 ggcagtatcgtgaattcgatgcAACACTCCCGTCGACAACAGA-3′) with SuperScript IV reverse tran-
552 scriptase (Life Technologies). RRV genomes were quantified by RT-qPCR using a tag sequence-
553 specific reverse primer (5′-GGCAGTATCGTGAATTCGATGC-3′) with a RRV sequence-specific
554 forward primer (5′-CCGTGGCGGGTATTATCAAT-3′) and an internal TaqMan probe (5′-
555 ATTAAGAGTG TAGCCATCC-3′), as previously described (Stoermer *et al*, 2012).
556
557 **Plaque Assay and Focus Formation Assay.** To quantify infectious virus, a plaque assay
558 or focus formation assay (FFA) were used as previously described (Hawman *et al.*, 2017). For
559 plaque assays, samples were serially diluted 10-fold in 1X PBS + 2% FBS + 1X $Ca^{2+}Mg^{2+}$ and
560 absorbed to BHK-21 cells in a 6-well plate for 1 h, after which cells were overlayed with 1%
561 immunodifusion agarose (MP Biomedical). After incubation at 37ºC for 40-44 h, cells were stained
562 with neutral red stain and plaques were counted. For the FFA, serum or tissue homogenate were

563 serially diluted 10-fold in 1X PBS+ 2% FBS+ 1X $Ca^{2+}Mg^{2+}$ and adsorbed to Vero cells in a 96-well
564 plate for 2 h. Cells were then overlaid with 0.5% methylcellulose in MEM-alpha + 10% FBS and
565 incubated at 37ºC for 18 h. Following fixation with 1% PFA, cells were probed with CHK-11
566 monoclonal antibody (Pal *et al*, 2013) at 500 ng/ml diluted in Perm Wash (1x PBS, 0.1% saponin,
567 0.1% BSA), followed by a secondary goat anti-mouse IgG conjugated to horseradish peroxidase
568 at 1:2,000 in Perm Wash. Foci were visualized with TrueBlue substrate (Fisher) and counted with
569 a CTL Biospot analyzer using Biospot software (Cellular Technology).
570
571 **Immunohistochemistry.** To evaluate KC depletion in the livers of DT-treated WT,
572 Clec4F-DTR^+, and CD169-DTR^+ mice and PLL- or CLL-treated WT mice, at the time of harvest
573 mice were perfused with 4% PFA and livers were harvested and fixed in 4% PFA for 24 h. Livers
574 were paraffin-embedded and immunohistochemistry was performed on 5-micrometer sections
575 using F4/80 antibody clone Cl:A3-1 (BioRad Cat. No. MCA497) and the VECTASTAIN Elite ABS
576 HRP kit (Vector Laboratories, PK-6100) as previously described (Carpentier *et al.*, 2019). To
577 quantify the efficiency of KC depletion, $F4/80^+$ cells were counted from 10 randomly selected high-
578 power fields (HPF; 40X) for each stained liver section, and were used to calculated the average
579 number of $F4/80^+$ cells per HPF of view.
580
581 **Isolation of cells from lymph nodes and flow cytometry.** To evaluate MARCO
582 expressing cells in lymphoid tissue, popliteal and inguinal lymph nodes were pooled from WT or
583 $MARCO^{-/-}$ mice. Lymph nodes were minced with a 22-gage needle in 1 mL of digestion media
584 (EHAA with 0.25 mg/mL Liberase DL and 17 µg/mL DNase) and incubated at 37°C for 1 h, after
585 which an equal volume of dissociation buffer (0.1M EDTA in EHAA) was added and incubated at
586 37°C for 5 min. Cells were passed through a 100 µm cell strainer (BD Falcon). Single-cell
587 suspensions were incubated for 20 min at 4°C with anti–mouse FcγRIII/II (2.4G2; BD

Pharmingen) prior to staining for 1 h at 4°C with the following antibodies from BioLegend (most) or Novus Biologicals (MARCO) diluted in FACS buffer (PBS with 2% FBS): anti-CD45 (30-F11), anti-PDPN (8.1.1), anti-CD31 (390), anti-CD169 (3D6.112), anti-CD11c (BV510), anti-CD11b (M1.70), anti-B220 (RA3-6B2), anti-TCRβ (H57-597), anti-F4/80 (BM8), anti-NK1.1 (PL136) and anti-MARCO (2359A). Cells were fixed overnight in 1× PBS/1% paraformaldehyde (PFA) and analyzed on a BD LSR Fortessa cytometer using FACSDiva software. Further analysis was performed using FlowJo software (Tree Star).

Immunofluorescence and confocal microscopy. Lymph nodes were fixed in 1 mL of phosphate buffer containing 0.1 M L-lysine, 2% PFA, and 2.1 mg/mL NaIO4 at pH 7.4 for 24 h at 4°C, followed by incubation in 30% sucrose phosphate-buffered solution for 48 h, then in 30% sucrose/PBS for 24 hr. LNs were then embedded in optimal-cutting-temperature medium (Electron Microscopy Sciences) and frozen in dry-ice-cooled isopentane. Eighteen-µm sections were cut on a Leica cryostat (Leica Microsystems). Sections were blocked with 5% goat, donkey, bovine, rat or rabbit serum and then stained with one or more of the following: B220 (clone RA3-6B2, ThermoFisher), Lyve-1 (clone ALY7, ThermoFisher), CD169 (clone 3D6.112, BioLegend) MARCO (clone ED31, BioRad), CD11b (clone M1/70, BioLegend) and mCherry (polyclonal, Novus Bio, Cat# NBP2-25157). Images were acquired using identical photomultiplier tube (PMT) and laser power settings on a Leica Stellaris confocal microscope (Leica). Confocal microscopy images were collected over the entire popliteal lymph node (representing approximately a 7 mm^2 imaged area) and individual fields (tiles) were merged into a single image file. Images were analyzed using Imaris v9.02 software (Oxford Instruments). Colocalization of Lyve1 and mCherry was performed using the Coloc module of Imaris (Oxford Instruments) and % of colocalized (double positive) voxels quantitated by the program using the same settings for each LN.

Preparation of single-cell suspensions for single-cell mRNA sequencing. The draining popliteal lymph node from mock- or CHIKV-inoculated mice were pooled into individual replicates (3 replicates; LNs from 5 mice pooled per replicate). Lymph nodes were mechanically homogenized using a 22G needle in Click's medium (Irvine Scientific, 9195) supplemented with 5 mg/mL liberase DL (Roche, 05401160001) and 2.5 mg/mL DNase (Roche 10104159001) for 1 h at 37°C. After incubation, digested tissues were clarified by passing through a 100 µm cell strainer. Cell suspensions were enriched for $CD45^-$ cells by labeling cells with PE-conjugated anti-mouse CD45 (30-F11), CD140A (APA5), and Ter119 (Ter119) monoclonal antibodies and subsequent depletion of PE-labeled cells using Miltenyi anti-PE microbeads (130-048-801) and Miltenyi MACS LS (130-042-401) columns according to the manufacturer's instructions with the following modifications: (1) we used 25% of the recommended volume of anti-PE microbeads and (2) we subjected the $CD45^-$ enriched cell fraction to a second MACS LS column. All cell suspensions post-column enrichment were enumerated using a hemacytometer. Cell fractions throughout the procedure were analyzed for PE-labeled cell depletion and enrichment of $CD45^-$ cells by flow cytometry. Cell fractions were stained with fixable LIVE/DEAD dye (Invitrogen, L34955) and antibodies against the following cell surface antigens: CD45 (30-F11), CD31 (390), PDPN (8.1.1), B220 (RA3-6B2), TCRβ (H57-597), CD11b (M1/70), and Ly6C (HK1.4). All flow cytometry antibodies from obtained from BioLegend, BD Bioscience or eBioscience. Following surface antigen staining, cells were washed, fixed in 1%PFA/1%FBS, and data was acquired on a BD LSR Fortessa X-20 flow cytometer. Data analysis was performed using FlowJo analysis software (Tree Star).

Single-cell library preparation using the 10x Genomics platform. Lymph node cell suspensions enriched for $CD45^-$ cells were subject to single-cell droplet-encapsulation using the Next GEM Chip G Kit (1000127) and a 10x Genomics chromium controller housed in our BSL3 laboratory. We targeted recovery of 10,000 cells for single-cell RNA sequencing for each

639 replicate. Single-cell gene expression libraries were generated using the Next GEM single-cell 3′
640 GEM library and gel bead kit v3.1 (1000128) and single index kit T set A (1000213) according to
641 the manufacturer's instructions (10x Genomics). Sequences were generated with the Illumina
642 NovaSEQ 6000 instrument using S4 flow cells and 300 cycle SBS reagents. We targeted 50,000
643 reads per cell, with sequencing parameters of Read 1:151 cycles; i7 index: 10 cycles; i5 index: 0
644 cycles; Read 2: 151 cycles.
645
646 **Transcriptome and oligonucleotide detection and analysis.** FASTQ files for each
647 replicate (3 mock, 3 CHIKV-infected) were processed using the cellranger count pipeline (v5.0.1).
648 Reads were aligned to the mm10 and CHIKV AF15561 (EF452493.1) reference genomes.
649 Analysis of gene expression data was performed using the Seurat R package (v4.0.0). Gene
650 expression data for each biological replicate were combined into a single Seurat object. CHIKV
651 counts were included as a separate "assay" in the Seurat object so they would not influence
652 downstream processing (dimensionality reduction, clustering) of the mouse gene expression
653 data.
654 CHIKV-low and -high cells were identified by first filtering cells to only include those with
655 >5 CHIKV counts. K-means clustering was then used to independently group each biological
656 replicate into CHIKV-low and -high populations (Walsh *et al.*, 2021). Cells with 5 CHIKV counts
657 or less were included in the CHIKV-low population. Cells were filtered based on the number of
658 detected mouse genes (>250 and <6000) and the percent mitochondrial counts (<20%). Genes
659 were filtered to only include those detected in >5 cells. Potential cell doublets were removed using
660 the DoubletFinder (v2.0.3) R package using an estimated doublet rate of 10%. Due to the ability
661 of CHIKV to inhibit host transcription (Fig. S8), CHIKV-high cells with a low number of detected
662 mouse genes (<250) or a high fraction of mitochondrial reads (>20%) were not filtered and
663 remained in the dataset for the downstream analysis. The fraction of CHIKV counts was
664 calculated by dividing the number of CHIKV counts by the total number of counts for each cell.

Mouse gene expression counts were normalized by the total mouse counts for the cell, multiplied by a scale factor (10,000), and log-transformed (NormalizeData), Normalized mouse counts were scaled and centered (ScaleData) using the top 2000 variable features (FindVariableFeatures). The scaled data were used for PCA (RunPCA) and the first 40 principal components were used to find clusters (FindNeighbors, FindClusters) and calculate uniform manifold approximation and projection (UMAP) (RunUMAP).

B cells and T cells were identified based on CD19 and CD3 expression, respectively. The remaining cell types were annotated using the R package clustifyr (https://rnabioco.github.io/clustifyr) with published reference RNA-seq data (Heng, 2008; Malhotra *et al.*, 2012; Rodda *et al.*, 2018) available for download through the clustifyrdata R package, https://rnabioco.github.io/clustifyrdata). Endothelial cells were further classified using reference data for mouse LEC subsets (Xiang *et al.*, 2020).

Statistical Analysis. Appropriate experimental sample sizes were determined using a power calculation (80% power, 0.05 type I error) to detect a 4-5-fold effect in pre-existing sample sets. Each Figure legend defines the biological replicates of individual mice (N) and the number of experiments performed. Data are represented as mean ± SD or mean ± SEM, as indicated. The statistical tests conducted on each data set are indicated in the Figure legend and were performed using GraphPad Prism 8.0. Two-sided t-tests (parametric) or Mann Whitney tests (nonparametric) were used to compare two groups. One-way ANOVA with Bonferroni's multiple comparison test (parametric) or Kruskal-Wallis with Dunn's multiple comparisons test (nonparametric) were used to compare three or more groups, and two-way ANOVA with Bonferroni's multiple comparison test was used to compare two groups at multiple time points.

Acknowledgements

This work was supported by Public Health Service grants R01 AI148144 and R01 AI141436 to T.E.M., F32 AI140567 to K.S.C., F32 AI122463 to M.K.M., T32 AI007405 to K.S.C., T32 AI074491 to R.M.S, and R35 GM119550 and R01 AG071467 to J.R.H.. H.D.H. is supported by the Intramural Research Program of NIAID, NIH (https://www.niaid.nih.gov/) and R.M.S is supported by the RNA Bioscience Initiative. The funders had no role in study design, data collection and analysis, decision to publish, or preparation of the manuscript.

Author Contributions

K.S.C., E.D.L., B.A.J.T., J.R.H., H.D.H., and T.E.M. designed the experiments. K.S.C., B.J.D., M.K.M., N.A.M, C.J.L, F.S.L., and G.V.R. performed the experiments. K.S.C., R.M.S., M.K.M., G.V.R., H.D.H., and T.E.M. performed the data analysis. K.S.C., R.M.S., and T.E.M. wrote the initial draft of the manuscript, with the other authors providing comments and edits to the final version.

Declaration of Interests

The authors declare no competing interests

References

Arredouani M, Yang Z, Ning Y, Qin G, Soininen R, Tryggvason K, Kobzik L (2004) The scavenger receptor MARCO is required for lung defense against pneumococcal pneumonia and inhaled particles. *The Journal of experimental medicine* 200: 267-272

Ashbrook AW, Burrack KS, Silva LA, Montgomery SA, Heise MT, Morrison TE, Dermody TS (2014) Residue 82 of the Chikungunya virus E2 attachment protein modulates viral dissemination and arthritis in mice. *Journal of Virology* 88: 12180-12192

716 Bellomo A, Gentek R, Bajenoff M, Baratin M (2018) Lymph node macrophages: Scavengers,
717 immune sentinels and trophic effectors. *Cell Immunol* 330: 168-174
718 Berendam SJ, Koeppel AF, Godfrey NR, Rouhani SJ, Woods AN, Rodriguez AB, Peske JD,
719 Cummings KL, Turner SD, Engelhard VH (2019) Comparative Transcriptomic Analysis Identifies
720 a Range of Immunologically Related Functional Elaborations of Lymph Node Associated
721 Lymphatic and Blood Endothelial Cells. *Front Immunol* 10: 816
722 Bilzer M, Roggel F, Gerbes AL (2006) Role of Kupffer cells in host defense and liver disease.
723 *Liver Int* 26: 1175-1186
724 Bogoslowski A, Kubes P (2018) Lymph Nodes: The Unrecognized Barrier against Pathogens.
725 *ACS Infect Dis* 4: 1158-1161
726 Borges da Silva H, Fonseca R, Pereira RM, Cassado AdA, Álvarez JM, D'Império Lima MR (2015)
727 Splenic Macrophage Subsets and Their Function during Blood-Borne Infections. *Frontiers in*
728 *Immunology* 6: 480
729 Borgherini G, Poubeau P, Jossaume A, Gouix A, Cotte L, Michault A, Arvin Berod C, Paganin F
730 (2008) Persistent arthralgia associated with chikungunya virus: a study of 88 adult patients on
731 reunion island. *Clinical Infectious Diseases* 47: 469-475
732 Bowdish DM, Sakamoto K, Kim MJ, Kroos M, Mukhopadhyay S, Leifer CA, Tryggvason K, Gordon
733 S, Russell DG (2009) MARCO, TLR2, and CD14 are required for macrophage cytokine responses
734 to mycobacterial trehalose dimycolate and Mycobacterium tuberculosis. *PLoS Pathog* 5:
735 e1000474
736 Bowdish DM, Sakamoto K, Lack NA, Hill PC, Sirugo G, Newport MJ, Gordon S, Hill AV, Vannberg
737 FO (2013) Genetic variants of MARCO are associated with susceptibility to pulmonary
738 tuberculosis in a Gambian population. *BMC medical genetics* 14: 47
739 Bowdish DME, Gordon S (2009) Conserved domains of the class A scavenger receptors:
740 evolution and function. *Immunological reviews* 227: 19-31

741 Cardona-Ospina JA, Villamil-Gómez WE, Jimenez-Canizales CE, Castañeda-Hernández DM,
742 Rodríguez-Morales AJ (2015) Estimating the burden of disease and the economic cost
743 attributable to chikungunya, Colombia, 2014. *Transactions of The Royal Society of Tropical*
744 *Medicine and Hygiene* 109: 793-802

745 Carpentier KS, Davenport BJ, Haist KC, McCarthy MK, May NA, Robison A, Ruckert C, Ebel GD,
746 Morrison TE (2019) Discrete viral E2 lysine residues and scavenger receptor MARCO are
747 required for clearance of circulating alphaviruses. *Elife* 8

748 Chen Y, Sankala M, Ojala JRM, Sun Y, Tuuttila A, Isenman DE, Tryggvason K, Pikkarainen T
749 (2006) A phage display screen and binding studies with acetylated low density lipoprotein provide
750 evidence for the importance of the scavenger receptor cysteine-rich (SRCR) domain in the ligand-
751 binding function of MARCO. *The Journal of biological chemistry* 281: 12767-12775

752 Chow A, Her Z, Ong EKS, Chen J-m, Dimatatac F, Kwek DJC, Barkham T, Yang H, Rénia L, Leo
753 YS *et al* (2011) Persistent arthralgia induced by Chikungunya virus infection is associated with
754 interleukin-6 and granulocyte macrophage colony-stimulating factor. *Journal of Infectious*
755 *Diseases* 203: 149-157

756 Couturier E, Guillemin F, Mura M, Léon L, Virion J-M, Letort M-J, De Valk H, Simon F, Vaillant V
757 (2012) Impaired quality of life after chikungunya virus infection: a 2-year follow-up study.
758 *Rheumatology (Oxford, England)* 51: 1315-1322

759 de St Maurice A, Harmon J, Nyakarahuka L, Balinandi S, Tumusiime A, Kyondo J, Mulei S,
760 Namutebi A, Knust B, Shoemaker T *et al* (2018) Rift valley fever viral load correlates with the
761 human inflammatory response and coagulation pathway abnormalities in humans with
762 hemorrhagic manifestations. *PLOS Neglected Tropical Diseases* 12: e0006460

763 De Togni P, Goellner J, Ruddle NH, Streeter PR, Fick A, Mariathasan S, Smith SC, Carlson R,
764 Shornick LP, Strauss-Schoenberger J *et al* (1994) Abnormal Development of Peripheral
765 Lymphoid Organs in Mice Deficient in Lymphotoxin *Science* 264: 703-707

766 Dorrington MG, Roche AM, Chauvin SE, Tu Z, Mossman KL, Weiser JN, Bowdish DM (2013)
767 MARCO is required for TLR2- and Nod2-mediated responses to Streptococcus pneumoniae and
768 clearance of pneumococcal colonization in the murine nasopharynx. *J Immunol* 190: 250-258
769 Duffy MR, Chen T-H, Hancock WT, Powers AM, Kool JL, Lanciotti RS, Pretrick M, Marfel M,
770 Holzbauer S, Dubray C *et al* (2009) Zika virus outbreak on Yap Island, Federated States of
771 Micronesia. *The New England journal of medicine* 360: 2536-2543
772 Elomaa O, Kangas M, Sahlberg C, Tuukkanen J, Sormunen R, Liakka A, Thesleff I, Kraal G,
773 Tryggvason K (1995) Cloning of a Novel Bacteria-Binding Receptor Structurally Related to
774 Scavenger Receptors and Expressed in a Subset of Macrophages. *Cell* 80: 603-609
775 Farrell HE, Davis-Poynter N, Bruce K, Lawler C, Dolken L, Mach M, Stevenson PG (2015) Lymph
776 Node Macrophages Restrict Murine Cytomegalovirus Dissemination. *J Virol* 89: 7147-7158
777 Fros JJ, Pijlman GP (2016) Alphavirus Infection: Host Cell Shut-Off and Inhibition of Antiviral
778 Responses. *Viruses* 8
779 Fu R, Gillen AE, Sheridan RM, Tian C, Daya M, Hao Y, Hesselberth JR, Riemondy KA (2020)
780 clustifyr: an R package for automated single-cell RNA sequencing cluster classification.
781 *F1000Res* 9: 223
782 Fujimoto N, He Y, D'Addio M, Tacconi C, Detmar M, Dieterich LC (2020) Single-cell mapping
783 reveals new markers and functions of lymphatic endothelial cells in lymph nodes. *PLoS Biol* 18:
784 e3000704
785 Ghosh S, Gregory D, Smith A, Kobzik L (2011) MARCO regulates early inflammatory responses
786 against influenza: a useful macrophage function with adverse outcome. *Am J Respir Cell Mol Biol*
787 45: 1036-1044
788 Gonzalez SF, Lukacs-Kornek V, Kuligowski MP, Pitcher LA, Degn SE, Kim YA, Cloninger MJ,
789 Martinez-Pomares L, Gordon S, Turley SJ *et al* (2010) Capture of influenza by medullary dendritic
790 cells via SIGN-R1 is essential for humoral immunity in draining lymph nodes. *Nat Immunol* 11:
791 427-434

792 Gray EE, Cyster JG (2012) Lymph node macrophages. *J Innate Immun* 4: 424-436

793 Gupta P, Lai SM, Sheng J, Tetlak P, Balachander A, Claser C, Renia L, Karjalainen K, Ruedl C
794 (2016) Tissue-Resident CD169(+) Macrophages Form a Crucial Front Line against Plasmodium
795 Infection. *Cell Rep* 16: 1749-1761

796 Hawman DW, Carpentier KS, Fox JM, May NA, Sanders W, Montgomery SA, Moorman NJ,
797 Diamond MS, Morrison TE (2017) Mutations in the E2 Glycoprotein and the 3′ Untranslated
798 Region Enhance Chikungunya Virus Virulence in Mice. *Journal of Virology* 91: 32-17

799 Hawman DW, Stoermer KA, Montgomery SA, Pal P, Oko L, Diamond MS, Morrison TE (2013)
800 Chronic Joint Disease Caused by Persistent Chikungunya Virus Infection Is Controlled by the
801 Adaptive Immune Response. *Journal of Virology* 87: 13878-13888

802 Heng TSP, M.W.; The Immunological Genome Project Consortium (2008) The Immunological
803 Genome Project: network of gene expression in immune cells. *Nature Immunology* 9: 1091-1094

804 Hickey MJ, Kubes P (2009) Intravascular immunity: the host–pathogen encounter in blood
805 vessels. *Nature Reviews Immunology* 9: 364-375

806 Hickman HD, Takeda K, Skon CN, Murray FR, Hensley SE, Loomis J, Barber GN, Bennink JR,
807 Yewdell JW (2008) Direct priming of antiviral CD8+ T cells in the peripheral interfollicular region
808 of lymph nodes. *Nat Immunol* 9: 155-165

809 High M, Cho H-Y, Marzec J, Wiltshire T, Verhein KC, Caballero MT, Acosta PL, Ciencewicki J,
810 McCaw ZR, Kobzik L *et al* (2016) Determinants of host susceptibility to murine respiratory
811 syncytial virus (RSV) disease identify a role for the innate immunity scavenger receptor MARCO
812 gene in human infants. *EBIOM* 11: 73-84

813 Iannacone M, Moseman EA, Tonti E, Bosurgi L, Junt T, Henrickson SE, Whelan SP, Guidotti LG,
814 von Andrian UH (2010) Subcapsular sinus macrophages prevent CNS invasion on peripheral
815 infection with a neurotropic virus. *Nature* 465: 1079-1083

816 Jalkanen S, Salmi M (2020) Lymphatic endothelial cells of the lymph node. *Nat Rev Immunol* 20:
817 566-578

818 Jenne CN, Kubes P (2013) Immune surveillance by the liver. *Nature Immunology* 14: 996-1006

819 Johnston LJ, Halliday GM, King NJ (2000) Langerhans cells migrate to local lymph nodes
820 following cutaneous infection with an arbovirus. *J Invest Dermatol* 114: 560-568

821 Junt T, Moseman EA, Iannacone M, Massberg S, Lang PA, Boes M, Fink K, Henrickson SE,
822 Shayakhmetov DM, Di Paolo NC *et al* (2007) Subcapsular sinus macrophages in lymph nodes
823 clear lymph-borne viruses and present them to antiviral B cells. *Nature* 450: 110-114

824 Jupille HJ, Oko L, Stoermer KA, Heise MT, Mahalingam S, Gunn BM, Morrison TE (2011)
825 Mutations in nsP1 and PE2 are critical determinants of Ross River virus-induced musculoskeletal
826 inflammatory disease in a mouse model. *Virology* 410: 216-227

827 Kastenmuller W, Torabi-Parizi P, Subramanian N, Lammermann T, Germain RN (2012) A
828 spatially-organized multicellular innate immune response in lymph nodes limits systemic
829 pathogen spread. *Cell* 150: 1235-1248

830 Kedl RM, Lindsay RS, Finlon JM, Lucas ED, Friedman RS, Tamburini BAJ (2017) Migratory
831 dendritic cells acquire and present lymphatic endothelial cell-archived antigens during lymph node
832 contraction. *Nature Communications*: 1-15

833 Lanciotti RSL, M.L.; Rwaguma, E.B.; Lutwama, J.J.; Kram, T.M.; Karabatos, N.; Cropp, B.C.;
834 Miller, B.R. (1998) Emergence of Epidemic O'nyong-nyong Fever in Uganda after a 35-Year
835 Absence: Genetic Characterization of the Virus. *Virology*: 258-268

836 Lao W, Kang H, Jin G, Chen L, Chu Y, Sun J, Sun B (2017) Evaluation of the relationship between
837 MARCO and CD36 single-nucleotide polymorphisms and susceptibility to pulmonary tuberculosis
838 in a Chinese Han population. 1-9

839 Lee W-Y, Moriarty TJ, Wong CHY, Zhou H, Strieter RM, van Rooijen N, Chaconas G, Kubes P
840 (2010) An intravascular immune response to Borrelia burgdorferi involves Kupffer cells and iNKT
841 cells. *Nature Publishing Group* 11: 295-302

842 Lewis SM, Williams A, Eisenbarth SC (2019) Structure and function of the immune system in the
843 spleen. *Science immunology* 4: eaau6085

844 Liu WJ, Rourke MF, Holmes EC, Aaskov JG (2011) Persistence of Multiple Genetic Lineages
845 within Intrahost Populations of Ross River Virus. *Journal of Virology* 85: 5674-5678
846 Ma M-J, Wang H-B, Li H, Yang J-H, Yan Y, Xie L-P, Qi Y-C, Li J-L, Chen M-J, Liu W *et al* (2011)
847 Genetic Variants in MARCO Are Associated with the Susceptibility to Pulmonary Tuberculosis in
848 Chinese Han Population. *PLoS ONE* 6: e24069-24066
849 MacDonald GHJ, R.E. (2000) Role of Dendritic Cell Targeting in Venezuelan Equine Encephalitis
850 Virus Pathogenesis. *Journal of Virology* 74: 914-922
851 MacLeod DT, Nakatsuji T, Wang Z, di Nardo A, Gallo RL (2015) Vaccinia virus binds to the
852 scavenger receptor MARCO on the surface of keratinocytes. *The Journal of investigative*
853 *dermatology* 135: 142-150
854 MacLeod DT, Nakatsuji T, Yamasaki K, Kobzik L, Gallo RL (2013) HSV-1 exploits the innate
855 immune scavenger receptor MARCO to enhance epithelial adsorption and infection. *Nature*
856 *Communications* 4: 1963
857 Maler MD, Nielsen PJ, Stichling N, Cohen I, Ruzsics Z, Wood C, Engelhard P, Suomalainen M,
858 Gyory I, Huber M *et al* (2017) Key Role of the Scavenger Receptor MARCO in Mediating
859 Adenovirus Infection and Subsequent Innate Responses of Macrophages. *mBio* 8: 855-815
860 Malhotra D, Fletcher AL, Astarita J, Lukacs-Kornek V, Tayalia P, Gonzalez SF, Elpek KG, Chang
861 SK, Knoblich K, Hemler ME *et al* (2012) Transcriptional profiling of stroma from inflamed and
862 resting lymph nodes defines immunological hallmarks. *Nat Immunol* 13: 499-510
863 McCarthy MK, Davenport BJ, Reynoso GV, Lucas ED, May NA, Elmore SA, Tamburini BA,
864 Hickman HD, Morrison TE (2018) Chikungunya virus impairs draining lymph node function by
865 inhibiting HEV-mediated lymphocyte recruitment. *JCI Insight* 3
866 Metsky HC, Matranga CB, Wohl S, Schaffner SF, Freije CA, Winnicki SM, West K, Qu J, Baniecki
867 ML, Gladden-Young A *et al* (2017) Zika virus evolution and spread in the Americas. *Nature* 546:
868 411-415

869 Miyake Y, Asano K, Kaise H, Uemura M, Nakayama M, Tanaka M (2007) Critical role of
870 macrophages in the marginal zone in the suppression of immune responses to apoptotic cell-
871 associated antigens. *J Clin Invest* 117: 2268-2278
872 Moro ML, Rezza G, Grilli E, Angelini R, Macini P, Spataro N, Gagliotti C, Massimiliani E, Sambri
873 V, Pierro AM *et al* (2010) Chikungunya Virus in North-Eastern Italy: A Seroprevalence Survey.
874 *The American Journal of Tropical Medicine and Hygiene* 82: 508-511
875 Musso D, Bossin H, Mallet HP, Besnard M, Broult J, Baudouin L, Levi JE, Sabino EC, Ghawche
876 F, Lanteri MC *et al* (2018) Zika virus in French Polynesia 2013-14: anatomy of a completed
877 outbreak. *The Lancet Infectious Diseases* 18: e172-e182
878 Pal P, Dowd KA, Brien JD, Edeling MA, Gorlatov S, Johnson S, Lee I, Akahata W, Nabel GJ,
879 Richter MK *et al* (2013) Development of a highly protective combination monoclonal antibody
880 therapy against Chikungunya virus. *PLoS Pathog* 9: e1003312
881 Pierson TC, Diamond MS (2018) The emergence of Zika virus and its new clinical syndromes.
882 *Nature* 560: 573-581
883 Pingen M, Bryden SR, Pondeville E, Schnettler E, Kohl A, Merits A, Fazakerley JK, Graham GJ,
884 McKimmie CS (2016) Host Inflammatory Response to Mosquito Bites Enhances the Severity of
885 Arbovirus Infection. *Immunity* 44: 1455-1469
886 Pozo-Aguilar JO, Monroy-Martínez V, Díaz D, Barrios-Palacios J, Ramos C, Ulloa-García A,
887 García-Pillado J, Ruiz-Ordaz BH (2014) Evaluation of host and viral factors associated with
888 severe dengue based on the 2009 WHO classification. *Parasites & vectors* 7: 590
889 Reynoso GV, Weisberg AS, Shannon JP, McManus DT, Shores L, Americo JL, Stan RV, Yewdell
890 JW, Hickman HD (2019) Lymph node conduits transport virions for rapid T cell activation. *Nat*
891 *Immunol* 20: 602-612
892 Rodda LB, Lu E, Bennett ML, Sokol CL, Wang X, Luther SA, Barres BA, Luster AD, Ye CJ, Cyster
893 JG (2018) Single-Cell RNA Sequencing of Lymph Node Stromal Cells Reveals Niche-Associated
894 Heterogeneity. *Immunity* 48: 1014-1028 e1016

Rodríguez-Morales AJ, Gil-Restrepo AF, Ramírez-Jaramillo V, Montoya-Arias CP, Acevedo-Mendoza WF, Bedoya-Arias JE, Chica-Quintero LA, Murillo-García DR, García-Robledo JE, Castrillón-Spitia JD *et al* (2016) Post-chikungunya chronic inflammatory rheumatism: results from a retrospective follow-up study of 283 adult and child cases in La Virginia, Risaralda, Colombia. *F1000Research* 5: 360

Schilte C, Staikowsky F, Staikovsky F, Couderc T, Madec Y, Carpentier F, Kassab S, Albert ML, Lecuit M, Michault A (2013) Chikungunya virus-associated long-term arthralgia: a 36-month prospective longitudinal study. *PLOS Neglected Tropical Diseases* 7: e2137

Scott CL, Zheng F, De Baetselier P, Martens L, Saeys Y, De Prijck S, Lippens S, Abels C, Schoonooghe S, Raes G *et al* (2016) Bone marrow-derived monocytes give rise to self-renewing and fully differentiated Kupffer cells. *Nat Commun* 7: 10321

Seiler P, Aichele P, Odermatt B, Hengartner H, Zinkernagel RM, Schwendener RA (1997) Crucial role of marginal zone macrophages and marginal zone metallophils in the clearance of lymphocytic choriomeningitis virus infection. *European Journal of Immunology* 27: 2626-2633

Soumahoro M-K, Boelle P-Y, Gaüzere B-A, Atsou K, Pelat C, Lambert B, La Ruche G, Gastellu-Etchegorry M, Renault P, Sarazin M *et al* (2011) The Chikungunya Epidemic on La Réunion Island in 2005–2006: A Cost-of-Illness Study. *PLOS Neglected Tropical Diseases* 5: e1197-1199

Stichling N, Suomalainen M, Flatt JW, Schmid M, Pacesa M, Hemmi S, Jungraithmayr W, Maler MD, Freudenberg MA, Pluckthun A *et al* (2018) Lung macrophage scavenger receptor SR-A6 (MARCO) is an adenovirus type-specific virus entry receptor. *PLoS Pathog* 14: e1006914

Stoermer KA, Burrack A, Oko L, Montgomery SA, Borst LB, Gill RG, Morrison TE (2012) Genetic Ablation of Arginase 1 in Macrophages and Neutrophils Enhances Clearance of an Arthritogenic Alphavirus. *The Journal of Immunology* 189: 4047-4059

Takeda A, Hollmen M, Dermadi D, Pan J, Brulois KF, Kaukonen R, Lonnberg T, Bostrom P, Koskivuo I, Irjala H *et al* (2019) Single-Cell Survey of Human Lymphatics Unveils Marked

Endothelial Cell Heterogeneity and Mechanisms of Homing for Neutrophils. *Immunity* 51: 561-572 e565

Tamburini BA, Burchill MA, Kedl RM (2014) Antigen capture and archiving by lymphatic endothelial cells following vaccination or viral infection. *Nature Communications* 5: 1161-1131

Thuong NT, Tram TT, Dinh TD, Thai PV, Heemskerk D, Bang ND, Chau TT, Russell DG, Thwaites GE, Hawn TR *et al* (2016) MARCO variants are associated with phagocytosis, pulmonary tuberculosis susceptibility and Beijing lineage. *Genes Immun* 17: 419-425

Van Rooijen N, Sanders A (1994) Liposome mediated depletion of macrophages: mechanism of action, preparation of liposomes and applications. *Journal of immunological methods* 174: 83-93

Vanlandingham DLT, K.; Klingler, K.A.; Hong, C.; Mcelroy, K.L.; Lehane, M.J.; Higgs, S. (2006) Determinants of Vector Specificity of O'nyong nyong and Chikungunya Viruses in Anopheles and Ades Mosquitoes. *Am J Trop Med Hyg* 74: 663-669

Vaughn DW, Green S, Kalayanarooj S, Innis BL, Nimmannitya S, Suntayakorn S, Endy TP, Raengsakulrach B, Rothman AL, Ennis FA *et al* (2000) Dengue viremia titer, antibody response pattern, and virus serotype correlate with disease severity. *Journal of Infectious Diseases* 181: 2-9

Vijayakumar K, George B, Anish TS, Rajasi RS, Teena MJ, Sujina CM (2013) Economic impact of chikungunya epidemic: out-of-pocket health expenditures during the 2007 outbreak in Kerala, India. *The Southeast Asian journal of tropical medicine and public health* 44: 54-61

Vokali E, Yu SS, Hirosue S, Rincon-Restrepo M, F VD, Scherer S, Corthesy-Henrioud P, Kilarski WW, Mondino A, Zehn D *et al* (2020) Lymphatic endothelial cells prime naive CD8(+) T cells into memory cells under steady-state conditions. *Nat Commun* 11: 538

Volk SM, Chen R, Tsetsarkin KA, Adams AP, Garcia TI, Sall AA, Nasar F, Schuh AJ, Holmes EC, Higgs S *et al* (2010) Genome-scale phylogenetic analyses of chikungunya virus reveal independent emergences of recent epidemics and various evolutionary rates. *Journal of Virology* 84: 6497-6504

946 Vuong NL, Quyen NTH, Tien NTH, Tuan NM, Kien DTH, Lam PK, Tam DTH, Van Ngoc T, Yacoub
947 S, Jaenisch T *et al* (2020) Higher plasma viremia in the febrile phase is associated with adverse
948 dengue outcomes irrespective of infecting serotype or host immune status: an analysis of 5642
949 Vietnamese cases. *Clin Infect Dis*
950 Waggoner JJ, Gresh L, Vargas MJ, Ballesteros G, Tellez Y, Soda KJ, Sahoo MK, Nuñez A,
951 Balmaseda A, Harris E *et al* (2016) Viremia and Clinical Presentation in Nicaraguan Patients
952 Infected With Zika Virus, Chikungunya Virus, and Dengue Virus. *Clinical Infectious Diseases* 63:
953 1584-1590
954 Walsh SM, Sheridan RM, Lucas ED, Doan TA, Ware BC, Schafer J, Fu R, Burchill MA,
955 Hesselberth JR, Tamburini BAJ (2021) Molecular tracking devices quantify antigen distribution
956 and archiving in the murine lymph node. *Elife* 10
957 Weaver SC (2018) Prediction and prevention of urban arbovirus epidemics: A challenge for the
958 global virology community. *ANTIVIRAL RESEARCH* 156: 80-84
959 Winkelmann ER, Widman DG, Xia J, Johnson AJ, van Rooijen N, Mason PW, Bourne N, Milligan
960 GN (2014) Subcapsular sinus macrophages limit dissemination of West Nile virus particles after
961 inoculation but are not essential for the development of West Nile virus-specific T cell responses.
962 *Virology* 450-451: 278-289
963 Xiang M, Grosso RA, Takeda A, Pan J, Bekkhus T, Brulois K, Dermadi D, Nordling S,
964 Vanlandewijck M, Jalkanen S *et al* (2020) A Single-Cell Transcriptional Roadmap of the Mouse
965 and Human Lymph Node Lymphatic Vasculature. *Front Cardiovasc Med* 7: 52
966 Zeller H, Van Bortel W, Sudre B (2016) Chikungunya: Its History in Africa and Asia and Its Spread
967 to New Regions in 2013–2014. *Journal of Infectious Diseases* 214: S436-S440
968 Zeng Z, Surewaard BGJ, Wong CHY, Geoghegan JA, Jenne CN, Kubes P (2016) CRIg Functions
969 as a Macrophage Pattern Recognition Receptor to Directly Bind and Capture Blood-Borne Gram-
970 Positive Bacteria. *Cell Host & Microbe* 20: 99-106

971 Zhang R, Earnest JT, Kim AS, Winkler ES, Desai P, Adams LJ, Hu G, Bullock C, Gold B, Cherry
972 S *et al* (2019) Expression of the Mxra8 Receptor Promotes Alphavirus Infection and Pathogenesis
973 in Mice and Drosophila. *Cell Rep* 28: 2647-2658 e2645
974 Zhang R, Kim AS, Fox JM, Nair S, Basore K, Klimstra WB, Rimkunas R, Fong RH, Lin H, Poddar
975 S *et al* (2018) Mxra8 is a receptor for multiple arthritogenic alphaviruses. *Nature* 557: 570-574
976
977
978
979
980
981
982
983
984
985
986
987
988
989
990
991
992
993
994
995
996

997 **Figure Legends**

998 **Figure 1. CHIKV infection outcomes are more severe in MARCO$^{-/-}$ mice and viremia**
999 **and dissemination are enhanced. (A-B)** WT or MARCO$^{-/-}$ C57BL/6 mice were inoculated
1000 subcutaneously (s.c.) in the left rear footpad with 10^3 PFU of CHIKV or CHIKV E2 K200R. The
1001 percent of starting body weight **(A)** and disease score (**B**) were recorded daily over 14 days. Mean
1002 ± SEM. N=7-12, three experiments. Two-way ANOVA with Bonferroni's multiple comparison test;
1003 ****$P < 0.0001$. (**C-E**) WT or MARCO$^{-/-}$ C57BL/6 mice were inoculated s.c. in the left rear footpad
1004 with 10^3 PFU of CHIKV. Serum collected on days 1, 2, 3, 5, 7, and 14 was analyzed by focus
1005 formation assay (FFA), mean ± SD **(C)** and by RT-qPCR, mean ± SD **(D)**. **(E)** Viral tissue burdens
1006 were analyzed at 1 day post inoculation (dpi) by FFA. Mean ± SEM. Two experiments, n=5-10.
1007 Two-way ANOVA with Bonferroni's multiple comparison test **(C-D**) or Mann-Whitney test **(E**);
1008 ****$P < 0.0001$. **(F-G)** WT or MARCO$^{-/-}$ C57BL/6 mice were inoculated s.c. in the left rear footpad
1009 with 10^3 PFU of ONNV **(F)** or RRV **(G).** Tissues and serum were collected at 1 dpi and analyzed
1010 by plaque assay. Mean ± SEM. Two experiments, n= 8-10. Mann-Whitney test; ****$P < 0.0001$.
1011
1012 **Figure 2. Depletion of Kupffer cells impedes CHIKV clearance from the circulation.**
1013 (**A)** WT and Clec4F-DTR$^+$ C57BL/6 mice were treated with diphtheria toxin (DT) either
1014 intraperitoneally (i.p.) 24 h prior to inoculation (n=10, two experiments, black dots) or intravenously
1015 (i.v.) 48 and 24 h prior to inoculation (n=4, one experiment, grey dots) to deplete KCs and
1016 inoculated i.v. with 10^8 CHIKV particles. Viral genomes in the inoculum and serum at 45 minutes
1017 (min)-post inoculation were determined by RT-qPCR. Mean ± SD. Three experiments, n= 14.
1018 Mann-Whitney test; ****$P < 0.0001$. (**B**) WT or Clec-4F-DTR$^+$ C57BL/6 mice were treated i.v. with
1019 DT, PLL or CLL prior to i.v. inoculation of 10^8 CHIKV particles. Viral genomes were quantified as
1020 in (A). Mean ± SD. One experiment, n=4. Mann-Whitney test; **$P < 0.01$, ****$P < 0.0001$. (**C**) WT

or CD169-DTR^{+} mice were treated i.p. with DT prior to i.v. inoculation of 10^{8} CHIKV particles. Viral genomes were quantified as in (A). Mean ± SD. Two experiments, n=7-8. Mann-Whitney test; ***$P < 0.001$. (**D**) Livers from WT, Clec4F-DTR^{+} or CD169-DTR^{+} mice treated i.p. with DT, or WT mice treated i.v. with PLL or CLL were analyzed by IHC to visualize F4/80^{+} macrophages (brown). Representative sections are shown. (**E**) F4/80^{+} cells in 10 randomly selected high-powered fields (HPF) per liver section were counted to calculate average F4/80^{+} cells per HPF. Mean ± SD. N=2-4 mice per group.

Figure 3. Depletion of KCs is not sufficient to enhance early CHIKV dissemination. (**A**) WT or Clec4F-DTR^{+} C57BL/6 mice were treated i.v. with DT prior to s.c. inoculation in the left rear footpad with 10^{3} PFU of CHIKV. Infectious virus was quantified at 24 hpi by FFA. Mean ± SEM. Two experiments, n=8. Mann-Whitney test; $P > 0.05$. (**B**) WT C57BL/6 mice were treated i.v. with PLL or CLL 42 h prior to s.c. inoculation in the left rear footpad with 10^{3} PFU of CHIKV. Infectious virus at 24 hpi was quantified by FFA. Mean ± SD. Two experiments, n=8. Mann-Whitney test; ***$P < 0.001$.

Figure 4. The draining lymph node limits arthritogenic alphavirus dissemination. (**A**) WT or LT$\alpha^{-/-}$ mice were treated i.v. with PLL or CLL 42 h prior to s.c. inoculation of the left rear footpad with 10^{3} PFU of CHIKV. Infectious virus at 24 hpi was analyzed by FFA. Mean ± SEM. Two experiments, n=8-10. Mann-Whitney test; *$P < 0.05$, ***$P < 0.001$, ****$P < 0.0001$. (**B**) WT or MARCO$^{-/-}$ C57BL/6 mice were inoculated s.c. in the left rear footpad with 10^{8} particles of WT CHIKV or CHIKV E2 K200R. Viral genomes in the dLN and serum at 2 hpi were quantified by RT-qPCR. Mean ± SD. Two experiments, n=10. Two-way ANOVA with Bonferroni's multiple comparisons test; ***$P < 0.001$, ****$P < 0.0001$. (**C**) WT or MARCO$^{-/-}$ C57BL/6 mice were

inoculated s.c. in the left rear footpad with 10^8 particles of RRV. Viral genomes in the dLN and serum were quantified by RT-qPCR. Mean ± SD. Two experiments, n=8-9. Mann-Whitney test; ***$P < 0.001$, ****$P < 0.0001$.

Figure 5. Macrophages in the dLN are not required for CHIKV accumulation in the dLN or limiting viral dissemination. (**A**) CD169-DTR$^+$ mice were treated i.p. with PBS or DT prior to collection of the popliteal LN. Frozen LN sections were stained for CD169$^+$ macrophages (green), B220$^+$ B cells (blue) or ERTR-7$^+$ stromal cells (red). (**B**) WT or CD169-DTR$^+$ C57BL/6 mice were treated i.p. with DT prior to s.c. inoculation in the left rear footpad with 10^8 particles of WT CHIKV. Viral genomes in the dLN and serum at 2 hpi were quantified by RT-qPCR. Mean ± SD. Two experiments, n=8. Mann-Whitney test; $P > 0.05$. (**C**) WT or CD169-DTR$^+$ C57BL/6 mice were treated i.p. with DT prior to s.c. inoculation in the left rear footpad with 10^3 PFU of CHIKV. Infectious virus at 24 hpi was quantified by FFA. Mean ± SEM. Two experiments, n=9-10. Mann-Whitney test; **$P < 0.01$.

Figure 6. MARCO$^+$ LECs capture lymph-borne CHIKV particles. WT or MARCO$^{-/-}$ C57BL/6 mice were inoculated s.c. in the rear feet with $5*10^4$ PFU of CHIKV-E2-mCherry and the popliteal dLNs were collected at 2 hpi. **(A)** Frozen dLN sections were stained for Lyve-1$^+$ LECs (white), MARCO (green), B220 (blue) and mCherry$^+$ CHIKV particles (red). **(B)** Representative histograms of confocal images showing voxel intensities for Lyve1 and mCherry. **(C)** Percent of Lyve1$^+$ voxels with mCherry signal; dots represent individual sections. **(D)** Higher magnification confocal image of a WT lymph node section stained as in (A) (**E**) Higher magnification confocal image of a MARCO$^{-/-}$ lymph node stained for CD11b$^+$ cells (white), mCherry$^+$ CHIKV particles

(red), B220^{+} B cells (blue), and CD169^{+} macrophages (green). Data are representative of 2 experiments, n=6-9. One-way ANOVA with Tukey's multiple comparisons test; ****P<0.0001.

Figure 7. MARCO^{+} LECs harbor CHIKV RNA . WT C57BL/6 mice were s.c. inoculated with PBS (mock, n=3) or 10^{3} PFU of CHIKV (n = 3) in the left rear footpad. At 24 hpi, the dLN was collected and enzymatically digested into a single cell suspension. Cells were enriched for CD45- cells and analyzed by scRNA-seq as described in the materials and methods. (**A**) UMAP projection shows each replicate for mock- and CHIKV-infected mice; the number of cells obtained for each replicate is shown at the bottom. (**B**) UMAP projection shows annotated cell types (top) and the proportion of cells identified for each cell type (bottom). (**C**) UMAP projection shows endothelial subtypes (top) and the proportion of cells identified for each cell type (bottom). Non-endothelial cells are shown in white. (**D**) UMAP projection shows Marco expression. (**E**) UMAP projection shows the fraction of counts that align to the CHIKV genome. (**F**) UMAP projection shows cell types for cells classified as CHIKV-high. CHIKV-low cells are shown in white. The proportion of CHIKV-high cells belonging to each cell type is shown on the right. (**G**) The fraction of counts that align to the CHIKV genome is shown for CHIKV-high cells. Only cell types that include >20 cells are shown. (**H, I**) MARCO (**H**) and Mxra8 (**I**) expression is shown for MARCO^{+} LECs for mock-infected cells and CHIKV-infected cells classified as either CHIKV-low or CHIKV-high. *P*-values were calculated using a two-sided Wilcoxon rank-sum test with Bonferroni correction.

Supplemental Figure Legends

Figure S1. CHIKV tissue burdens in distal tissues are enhanced in MARCO$^{-/-}$ mice at days 3, 7 and 14 pi. (A-C) WT or MARCO$^{-/-}$ C57BL/6 mice were inoculated subcutaneously in the left rear footpad with 10^3 PFU of CHIKV. Viral tissue burdens were analyzed at 3 **(A)**, 7 **(B)** and 14 **(C)** days post inoculation (dpi) by FFA (A), or RT-qPCR (B and C). Mean ± SEM Two experiments for each time point, n= 10. Mann-Whitney test; *P < 0.05, ***P < 0.001, ****P < 0.0001.

Figure S2. MARCO is expressed by medullary sinus macrophages and LECs in LNs. LNs were pooled from uninfected WT or MARCO$^{-/-}$ C57BL/6 mice. Representative flow plots and percentages of MARCO expressing cells by resident macrophage populations (A, C) and stromal cell populations (B, D) are shown. Mean ± SEM. Two experiments, n=4-5. Two-way ANOVA with Bonferroni's multiple comparisons test; **P < 0.01, ****P < 0.0001.

Figure S3. Depletion of phagocytic cells in the lymph node and liver does not enhance CHIKV dissemination. WT C57BL/6 mice were i.v. injected with PLL or CLL 42 h prior to virus inoculation and subcutaneously injected in the left rear footpad (FP) with PLL or CLL 24 h prior to virus inoculation as indicated. Mice were then inoculated s.c. with 10^3 PFU of CHIKV in the left rear footpad, and tissues and serum were collected at 24 hpi. Infectious virus was quantified by FFA. Mean ± SEM. Two experiment, n=8. Two-way ANOVA with Bonferroni's multiple comparison test, comparing all groups to IV PLL+ FP PLL group; **P < 0.01, ****P < 0.0001.

Figure S4. CHIKV-E2 mCherry is susceptible to clearance by a poly(I) sensitive scavenger receptor. WT C57BL/6 mice were treated i.v. with poly(C) or poly(I) 5 min prior to i.v.

1118 inoculation of 10^8 particles of CHIKV-E2 mCherry. Genomes in the inoculum and serum at 45 min
1119 post-inoculation were quantified by RT-qPCR. Mean ± SD. N=3, one experiment.
1120
1121 **Figure S5. CD45$^-$ cell enrichment.** Pre- and Post-CD45$^+$ cell depletion cell populations
1122 were analyzed by flow cytometry. (**A**) Representative plots of gating strategy used. (**B-C**)
1123 Representative flow plots of cell viability **(B**) and CD45$^+$ and CD45$^-$ cell populations (**C**) in pre-
1124 and post depleted postulations. **(D**) Percentages of CD45$^+$ and CD45$^-$ subsets among replicates.
1125 One experiment, n=3.
1126
1127 **Figure S6. LEC Annotations.** To assess the accuracy of endothelial cell type
1128 annotations, the subtype assignments were compared back to the reference data. The correlation
1129 with the reference RNA-seq data is shown for each subtype. Correlation coefficients (Spearman)
1130 are shown for each subtype.
1131
1132 **Figure S7. CHIKV-high classification and gene expression among CHIKV-high and**
1133 **CHIKV low cells. (A)** To identify cells with high amounts of viral RNA, cells were first filtered to
1134 only include those with >5 CHIKV counts. K-means clustering was then used to independently
1135 group each biological replicate into CHIKV-low and -high populations. Cells with <=5 CHIKV
1136 counts are included in the CHIKV-low group. CHIKV counts are shown below for each sample
1137 before filtering low quality cells (this includes all captured cells). **(B)** Cell quality metrics are shown
1138 for CHIKV-low and CHIKV-high cells for each replicate. These plots include all captured cells
1139 before quality filtering. CHIKV-high cells have fewer expressed mouse genes and an increased
1140 percentage of mitochondrial counts.
1141
1142

Figure 1

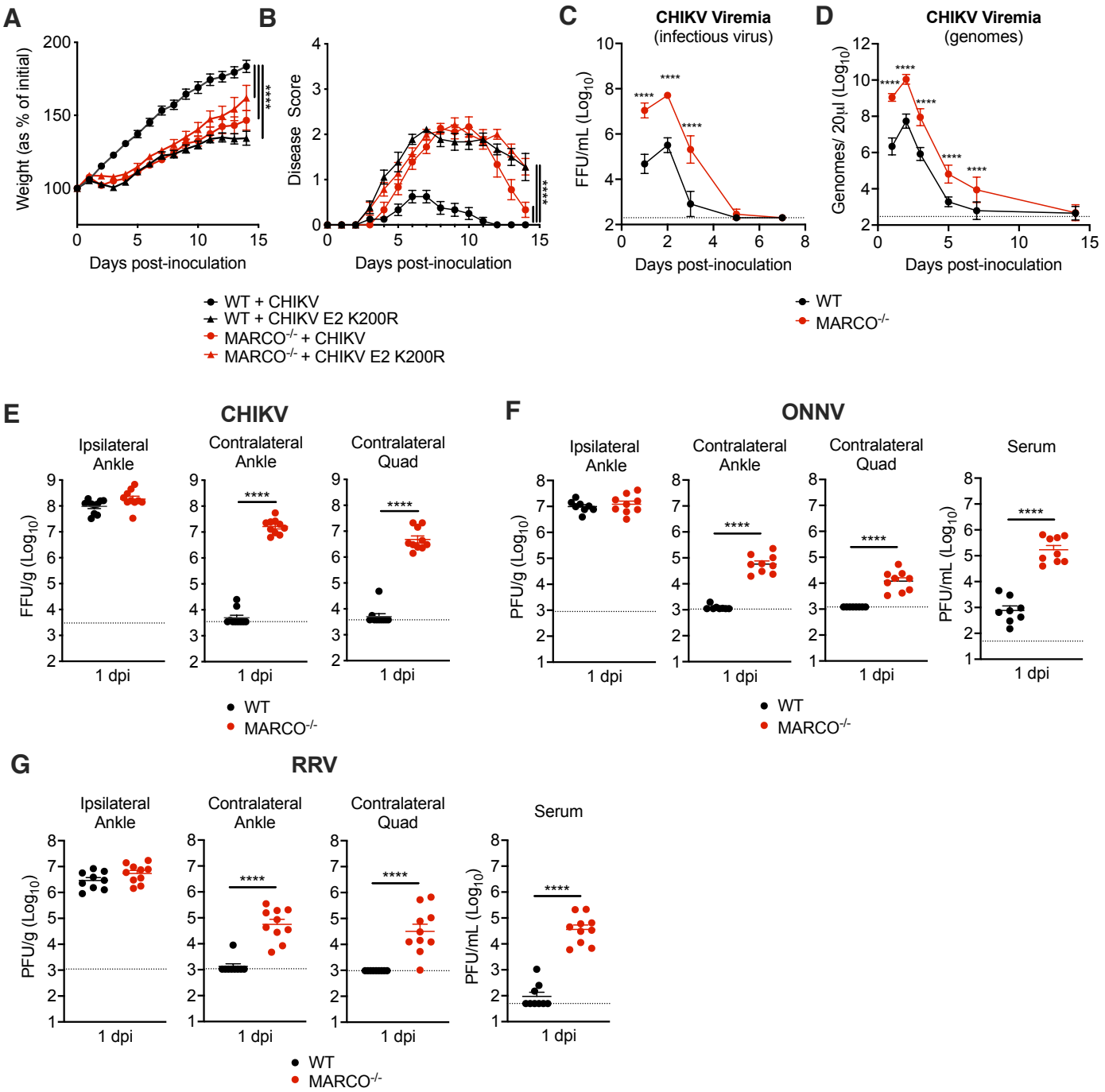
A
Weight (as % of initial)
Days post-inoculation
****
B
Disease Score
Days post-inoculation
****
C
CHIKV Viremia
(infectious virus)
FFU/mL (Log10)
Days post-inoculation
D
CHIKV Viremia
(genomes)
Genomes/ 20µl (Log10)
Days post-inoculation
WT + CHIKV
WT + CHIKV E2 K200R
MARCO-/- + CHIKV
MARCO-/- + CHIKV E2 K200R
WT
MARCO-/-
E
CHIKV
Ipsilateral Ankle
Contralateral Ankle
Contralateral Quad
FFU/g (Log10)
1 dpi
F
ONNV
Ipsilateral Ankle
Contralateral Ankle
Contralateral Quad
Serum
PFU/g (Log10)
PFU/mL (Log10)
1 dpi
G
RRV
Ipsilateral Ankle
Contralateral Ankle
Contralateral Quad
Serum
PFU/g (Log10)
PFU/mL (Log10)
1 dpi

Figure 2

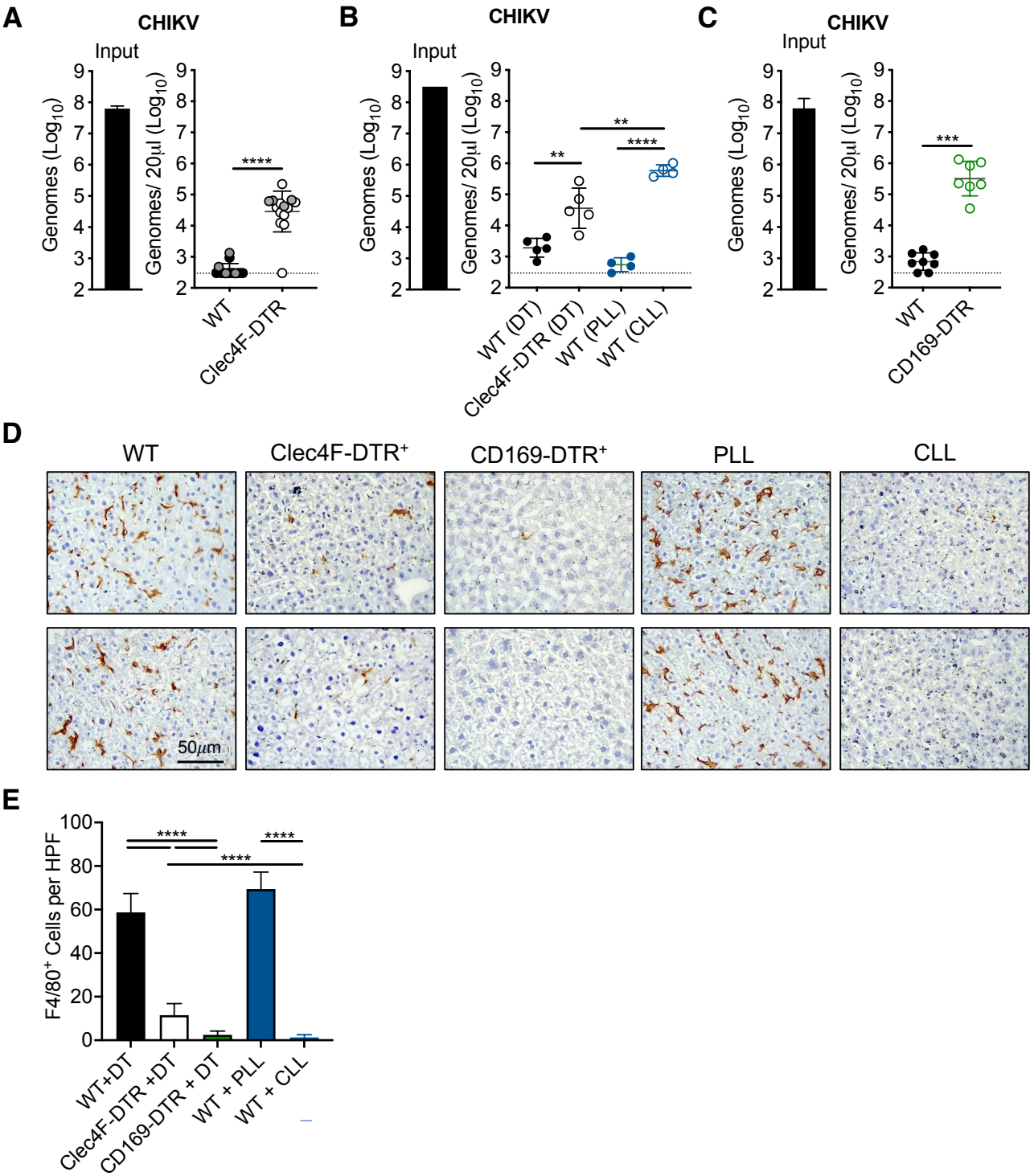
A
CHIKV
Input
Genomes (Log10)
Genomes/ 20µl (Log10)
****
WT
Clec4F-DTR
B
CHIKV
Input
**
****
WT (DT)
Clec4F-DTR (DT)
WT (PLL)
WT (CLL)
C
CHIKV
Input
***
WT
CD169-DTR
D
WT
Clec4F-DTR+
CD169-DTR+
PLL
CLL
50µm
E
F4/80+ Cells per HPF
****
WT+DT
Clec4F-DTR +DT
CD169-DTR + DT
WT + PLL
WT + CLL

Figure 3

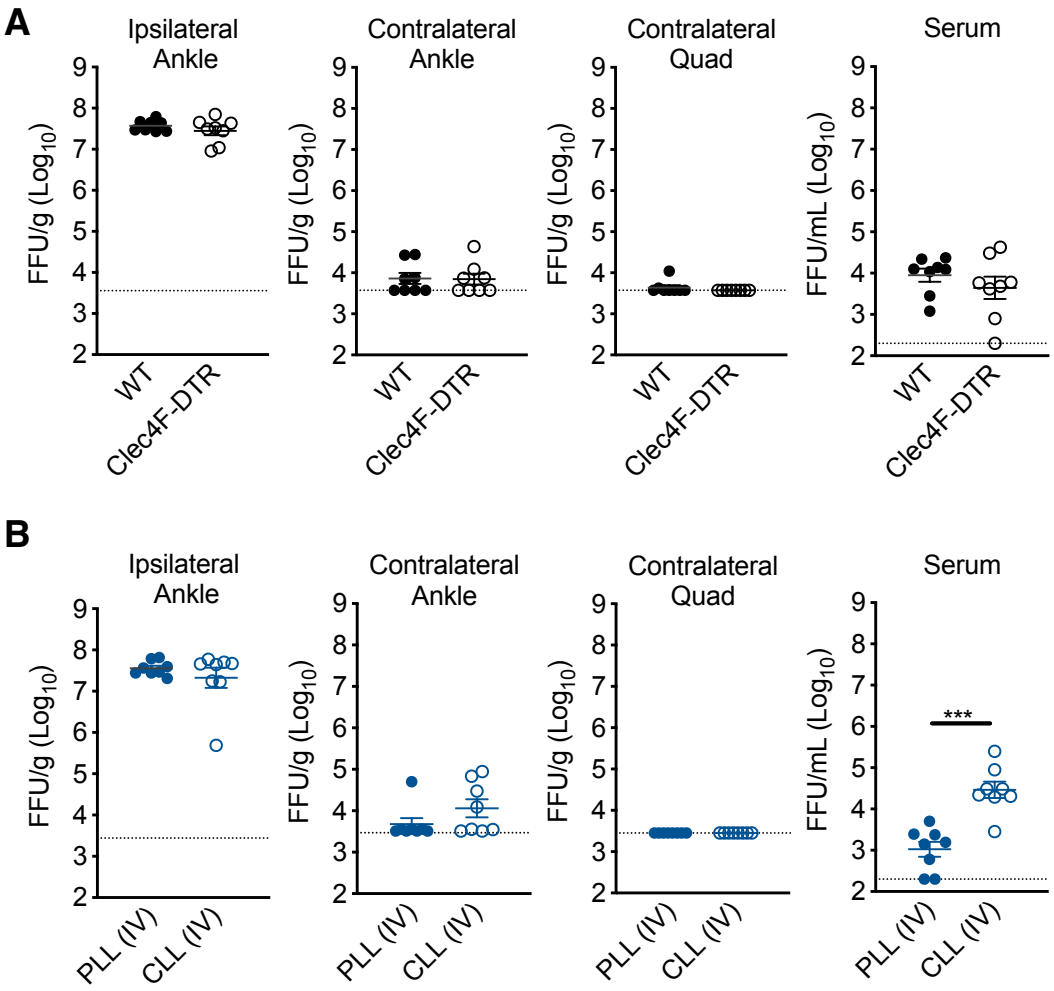
A
Ipsilateral Ankle
Contralateral Ankle
Contralateral Quad
Serum
FFU/g (Log10)
FFU/mL (Log10)
WT
Clec4F-DTR
B
PLL (IV)
CLL (IV)
***

Figure 4

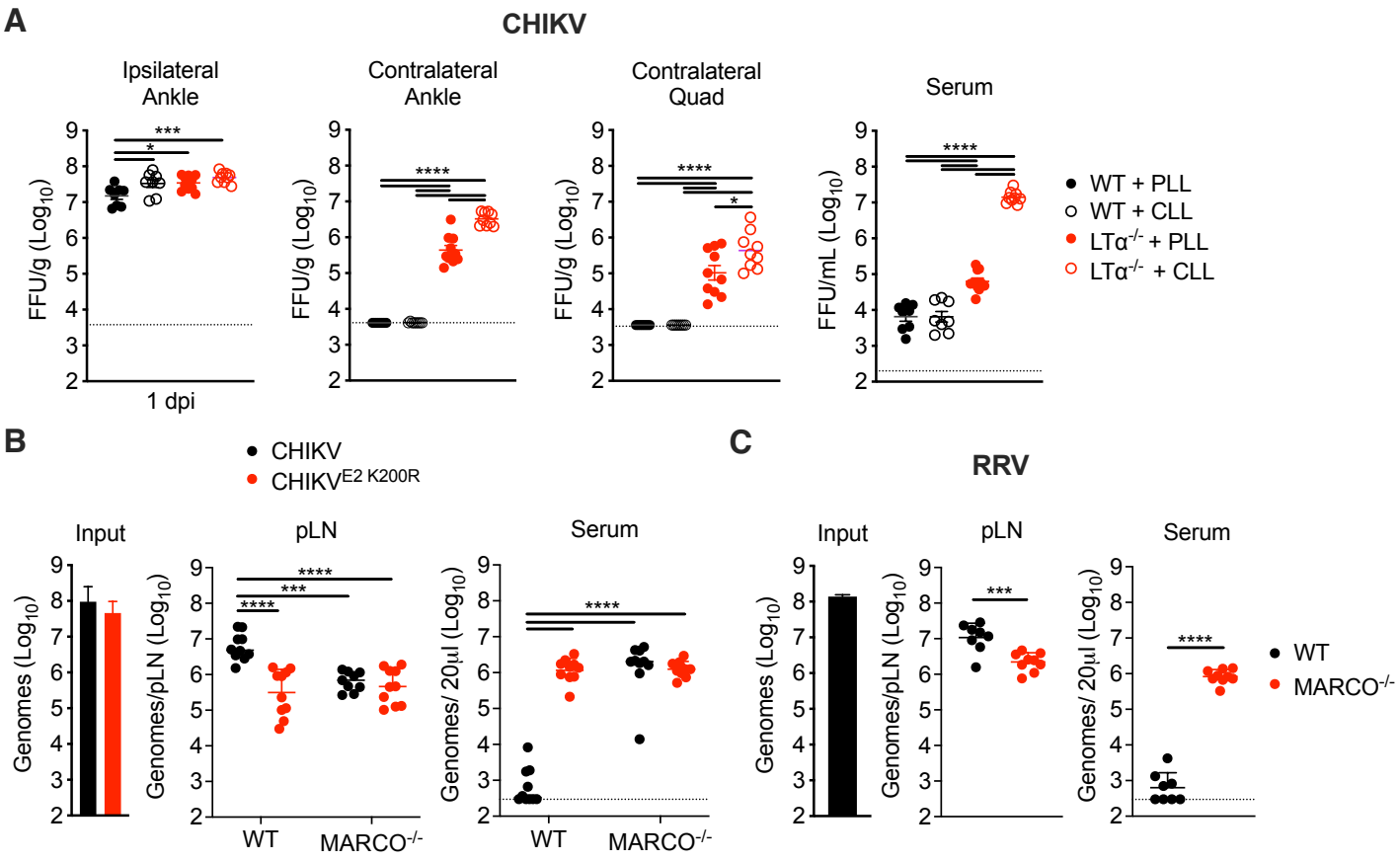
A
CHIKV
Ipsilateral Ankle
Contralateral Ankle
Contralateral Quad
Serum
FFU/g (Log10)
FFU/mL (Log10)
1 dpi
WT + PLL
WT + CLL
LTα-/- + PLL
LTα-/- + CLL
B
CHIKV
CHIKVE2 K200R
Input
pLN
Serum
Genomes (Log10)
Genomes/pLN (Log10)
Genomes/ 20µl (Log10)
WT
MARCO-/-
C
RRV
Input
pLN
Serum
WT
MARCO-/-

Figure 5

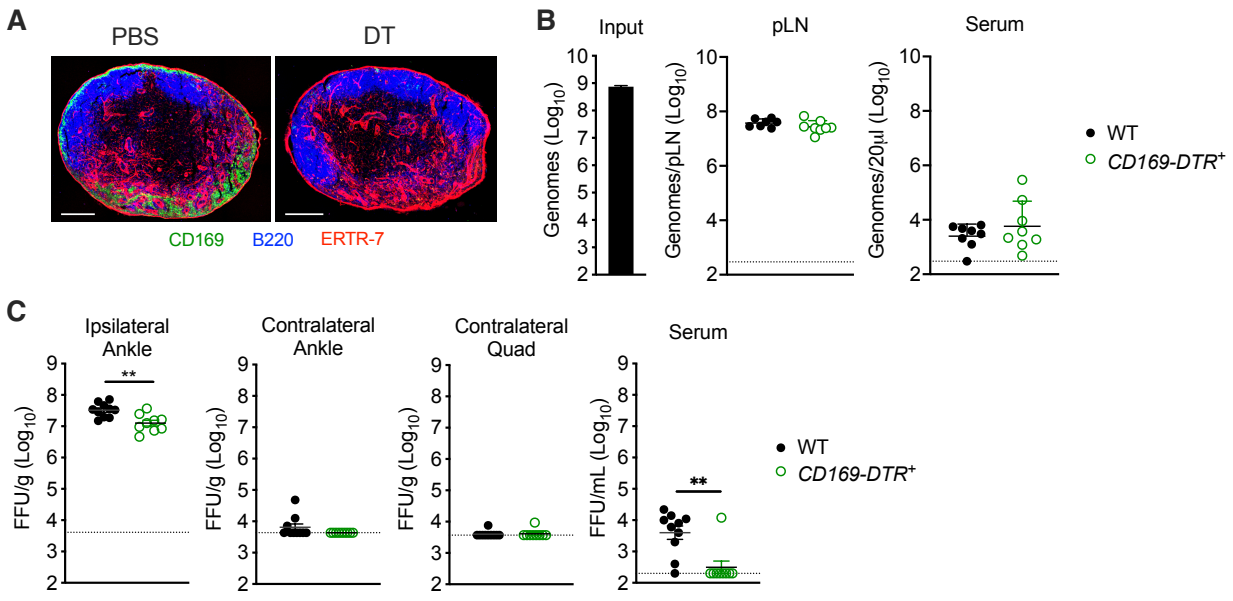
A
PBS
DT
CD169
B220
ERTR-7
B
Input
pLN
Serum
Genomes (Log10)
Genomes/pLN (Log10)
Genomes/20µl (Log10)
WT
CD169-DTR+
C
Ipsilateral Ankle
Contralateral Ankle
Contralateral Quad
Serum
FFU/g (Log10)
FFU/mL (Log10)
**
**
WT
CD169-DTR+

Figure 6

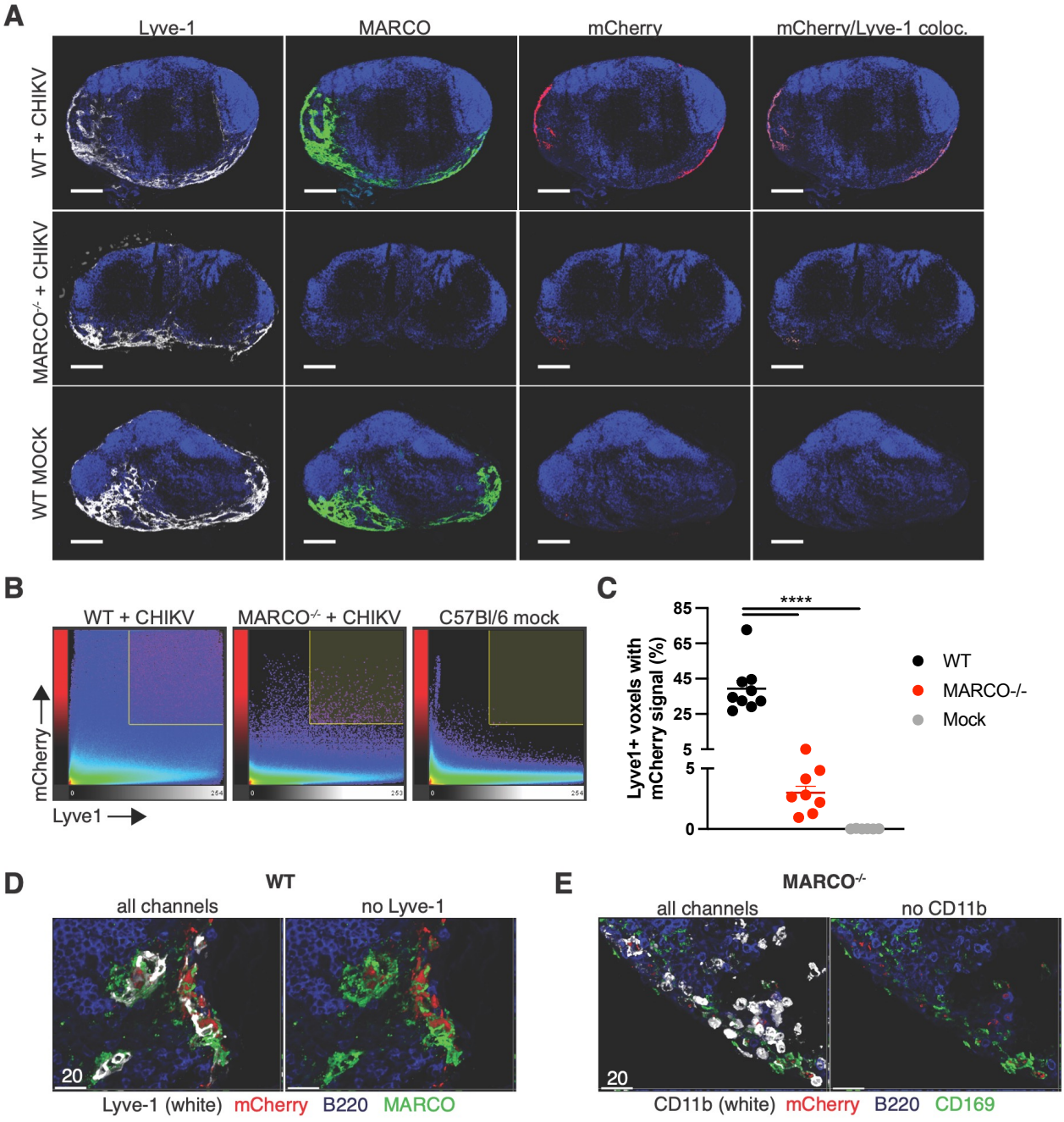
A
Lyve-1
MARCO
mCherry
mCherry/Lyve-1 coloc.
WT + CHIKV
MARCO-/- + CHIKV
WT MOCK
B
WT + CHIKV
MARCO-/- + CHIKV
C57Bl/6 mock
mCherry
Lyve1
C
****
Lyve1+ voxels with mCherry signal (%)
85
65
45
25
5
5
0
WT
MARCO-/-
Mock
D
WT
all channels
no Lyve-1
20
Lyve-1 (white) mCherry B220 MARCO
E
MARCO-/-
all channels
no CD11b
20
CD11b (white) mCherry B220 CD169

Figure 7

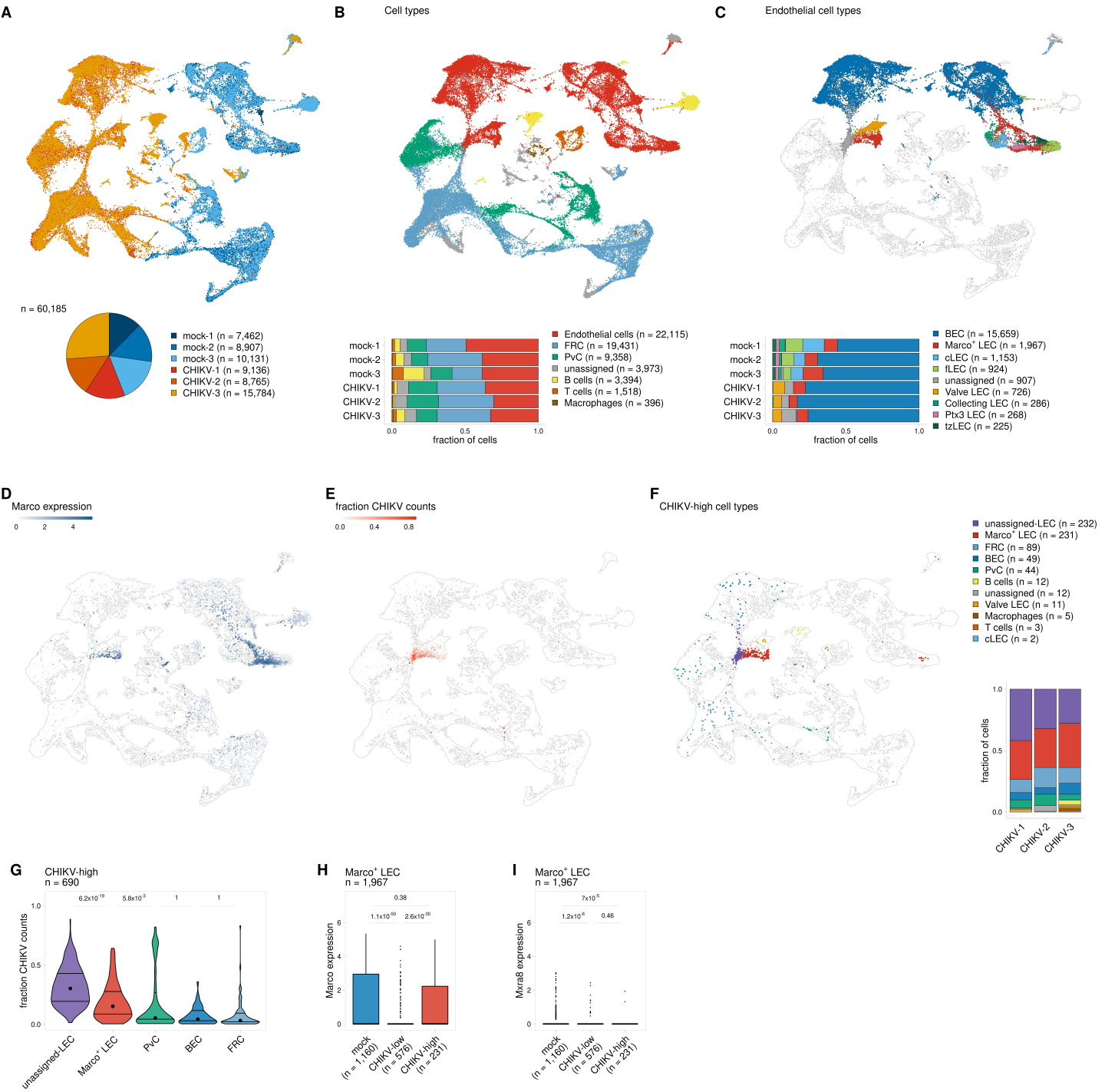
A
n = 60,185
mock-1 (n = 7,462)
mock-2 (n = 8,907)
mock-3 (n = 10,131)
CHIKV-1 (n = 9,136)
CHIKV-2 (n = 8,765)
CHIKV-3 (n = 15,784)
B
Cell types
mock-1
mock-2
mock-3
CHIKV-1
CHIKV-2
CHIKV-3
0.0
0.5
1.0
fraction of cells
Endothelial cells (n = 22,115)
FRC (n = 19,431)
PvC (n = 9,358)
unassigned (n = 3,973)
B cells (n = 3,394)
T cells (n = 1,518)
Macrophages (n = 396)
C
Endothelial cell types
BEC (n = 15,659)
Marco+ LEC (n = 1,967)
cLEC (n = 1,153)
fLEC (n = 924)
unassigned (n = 907)
Valve LEC (n = 726)
Collecting LEC (n = 286)
Ptx3 LEC (n = 268)
tzLEC (n = 225)
D
Marco expression
0
2
4
E
fraction CHIKV counts
0.0
0.4
0.8
F
CHIKV-high cell types
unassigned-LEC (n = 232)
Marco+ LEC (n = 231)
FRC (n = 89)
BEC (n = 49)
PvC (n = 44)
B cells (n = 12)
unassigned (n = 12)
Valve LEC (n = 11)
Macrophages (n = 5)
T cells (n = 3)
cLEC (n = 2)
fraction of cells
CHIKV-1
CHIKV-2
CHIKV-3
G
CHIKV-high
n = 690
fraction CHIKV counts
6.2x10-19
5.8x10-3
1
1
unassigned-LEC
Marco+ LEC
PvC
BEC
FRC
H
Marco+ LEC
n = 1,967
Marco expression
0.38
1.1x10-50
2.6x10-30
mock (n = 1,160)
CHIKV-low (n = 576)
CHIKV-high (n = 231)
I
Marco+ LEC
n = 1,967
Mxra8 expression
7x10-5
1.2x10-6
0.46
mock (n = 1,160)
CHIKV-low (n = 576)
CHIKV-high (n = 231)